Comparison of SCOPE simulated terrestrial chlorophyll fluorescence to HYPLANT measurements in Germany

XUANLU GAO
02, 2016

Supervisors
Dr. Christiaan van der Tol, Water resource department
Prof. Dr. Wouter Verhoef, Water resource department

External Examiner
Dr. Anke Schickling

Comparison of SCOPE simulated terrestrial chlorophyll fluorescence to HYPLANT measurements in Germany

XUANLU GAO
Enschede, The Netherlands, [02, 2016]

ABSTRACT

The problem I am trying to solve in this paper is to look for added value of SIF measurement data, and to analyze spatial variability feature of SIF at two peaks in HYPLANT.

The approach I adopt to solve the problem is by comparing modelled and measured SIF at 680 nm and 760 nm for different spatial variability feature of SIF and multi-time in one day. There are two types of datasets representing spatial variability features in HYPLANT SIF data: different land covers and transient area inside one land cover which have obvious SIF variability. Multi-time in one day include local time at 11:56, 13:50 and 16:05. For each dataset type, simulation and comparison steps are as follow: First vegetation parameters were retrieved by RTM model from reflectance spectra of HYPLANT; SIF spectra were simulated by SCOPE model with vegetation parameters as input data; then comparison were made between modelled and measured SIF at 680 nm and 760 nm.

The results obtained in this research include comparison between measured and modelled SIF for 5 land covers which are sugar beet, corn, potato, tree and grass at 680 nm and 760 nm, comparison between measured and modelled SIF in transient area in sugar beet at 680 nm and 760 nm, comparison between measured and modelled SIF for multi time in one day at 680 nm and 760 nm, SIF distribution at 680 nm and 760 nm for different land covers, SIF variability in transient area at 680 nm and 760 nm.

The obtained results can show added value of SIF include: SIF are unique when compared with reflectance, because there are low relations between modelled and measured SIF, especially at 680 nm. And SIF can provide more additional value of plant than reflectance data, because variations of modelled SIF are lower that measured SIF for nearly all situations. Also, SIF variability for different land covers and transient area are shown. Land covers have certain and specific distribution in plot which SIF at 680 versus SIF at 760. Changing trend of SIF at 680 are different from changing trend of SIF at 760 nm. When SIF at 760 nm have obvious decrease, SIF at 680 nm remain random fluctuations.

Acknowledgement

I want to thank my supervisors gratefully, Mr. van der Tol and Mr. Verhoef, for your patience and very professional attitudes.

I want to thank my parents and family, for your unconditional support and love.

I want to thank my friends for accompanying me all the way.

Siyuan, I finally submit this.

CONTENTS

LIST OF FIGURES

LIST OF TABLES

1. INTRODUCTION

1.1. Background

Plant produce sugars from carbon dioxide and water by harvesting sunlight. Sugar is the primary energy source for all life on earth (Luis Guanter, Zhang, Jung, Joiner, Voigt, et al., 2014). Hence growth of plants plays an important role on global carbon cycle and land surface ecosystem functioning. It is estimated that we must double world food production by 2050 to meet increasing demand. The quantity of photosynthesis places an upper limit on the supply of food and fuels in our agricultural systems (Tilman, Balzer, Hill, & Befort, 2011). Methods used to understand and model spatial global gross primary production (GPP, which means ecosystem gross photosynthesis) have limits of uncertainties because of complexity of the photosynthesis process. Remote sensing reflectance-based vegetation parameters can be used to monitor the vegetation condition, but estimation of GPP from vegetation parameters requires additional data and modeling steps, which both associated with considerable uncertainties (Luis Guanter, Zhang, Jung, Joiner, Voigt, et al., 2014).

In recent years, chlorophyll fluorescence has been used as a new indicator of photosynthesis. It has been indicated that chlorophyll fluorescence data can help improve models to have more accurate projections of agriculture productivity and productivity variations due to climate change (Luis Guanter, Zhang, Jung, Joiner, Voigt, et al., 2014). Chlorophyll fluorescence is an energy flux in the red and far-red region (650-800 nm) of the electromagnetic spectrum, and it is emitted by the photosynthesis II (PSII) of the chlorophyll molecules. It consists information about light harvest and photo transport of photosynthesis process. The direct relation between chlorophyll fluorescence and status of photosynthesis makes chlorophyll fluorescence a reasonable indicator for photosynthesis process.

Many ways to acquire chlorophyll fluorescence data exist. Chlorophyll fluorescence in algae and plants can be measured in controlled situations with artificial light instead of sunlight to evaluate PSII photochemistry (Baker, 2008). The results of this active method can be relatively accurate, but this method is costly, time consuming and it provides only point data. Due to geographical spatial distribution differences, spatially distributed data of solar induced chlorophyll fluorescence (SIF) are required to solve realistic regional or global issues.

Remote sensing technology can retrieve SIF map data in certain spatial resolution and temporal resolution with Fraunhofer Line Depth method (Meroni et al., 2009). First global satellite maps of SIF were acquired by Japanese satellite GOSAT with resolution in $2°*2°$ grids at 755 nm (Frankenberg et al., 2011). Later an improved method was developed to increase SIF results' accuracy and precision from Global Ozone Monitoring Instrument 2 (GOME 2) (Joiner et al., 2013). This method contributes to improved accuracy of SIF results which can be retrieved from moderate spectral resolution measurements like satellite GOSAT or GOME 2. But both GOSAT and GOME 2 are not designed for measurement of fluorescence but for atmospheric trace gas, also the coarse spatial and temporal resolution limit the application and further research of SIF data.

Airborne based imaging spectrometers can observe SIF data in intermediate spatial resolution. Maps of SIF were made from imaging spectrometer HYPLANT in Germany (Rascher et al., 2015). HYPLANT was specifically designed to detect vegetation and retrieve fluorescence. It consists of two modules on a single rack. One module provides surface radiance from 380 to 2500 nm in spectrum, and the other module provides surface radiance in the red and far-red spectrum with spectral resolution of 0.25 nm. The second module is designed to retrieve SIF between 670 and 780 nm (Rascher et al., 2015). The SIF data can be first acquired in physical units with about 10% error. It is not feasible to get global SIF data with airborne based spectrometers.

The Fluorescence Explorer (FLEX) which proposed by European Space Agency is under development to retrieve chlorophyll fluorescence in O_2 A- and B- bands (L. Guanter et al., 2010). This emission will improve spatial and temporal resolution of SIF map by carrying hyperspectral detecting instrument.

Soil-Canopy Observation of Photosynthesis and Energy fluxes (SCOPE) is a model which is been used to simulate SIF recently, and to retrieve information from SIF. In this model, scattering and absorption of light by leaves are calculated, especially the emission, scattering and absorption of fluorescence. Because of uncertainties of common models and complexity of SCOPE, systematic errors and sensitive parameters are issues to be focused on. Irradiance, leaf composition, leaf area index and the carboxylation capacity V_{cmo} are the most sensitive parameters affecting signal of SIF (Verrelst, Rivera, et al., 2015).

1.2.   Problem definition

Because of direct physical relation between photosynthesis process and SIF signal, SIF is regarded as a reasonable indicator of photosynthesis and GPP. It is found that monthly mean GPP at cropland flux tower sites and SIF have linear relations at US Corn Belt and grassland in Western Europe(Luis Guanter, Zhang, Jung, Joiner, & Voigt, 2014). But those relations were found by linear regression method which lack of physical process and base. Researches about SIF are relatively new, and it is not exactly known what the additional value of SIF is compared to reflectance data.

1.3.   Objectives

According to the problems definition above, the corresponding objectives have been defined.

Because the additional value of SIF compared to reflectance is not exactly known, therefore comparison between simulated SIF from reflectance and measured SIF will help to fill this knowledge gap. Vegetation parameters can be retrieved from reflectance by inversion of radiative transfer model (RTM), and then vegetation parameters will be used to simulate SIF spectrum with SCOPE model. If modelled SIF can reproduce the same data as measured SIF, then it means that reflectance data include vegetation information of SIF. If modelled SIF cannot reproduce the measured SIF, then

additional information can be understood by analyzing differences of two data sources, notably the measured and the simulated SIF.

Thus the main objective is to test whether there is any added value of SIF compared to reflectance.

To test whether simulated SIF is equal to measured SIF for different spatial variability features and for multi-time in one day.
To analyze the differences between simulated and measured SIF for different spatial variability features and for multi-time in one day.
To look for relations between simulated and measured SIF for different spatial variability features and for multi-time in one day.

Secondly reflectance and SIF data with obvious spatial variability from HYPLANT will be used as main data source. Spatial variability feature of SIF and the corresponding modelling result will be analyzed.

Thus the second objective is to analyze spatial variability of simulated and measured SIF.

To analyze spatial variability feature of SIF data from HYPLANT.
To analyze relation between SIF data at 680 nm and 760 nm for each variability feature.

2. LITERATURE

This chapter reviews three topics: (1) the relationships between vegetation parameters and the growing cycle of the crop and relations between chlorophyll fluorescence and plant growing, (2) relations between vegetation parameters and reflectance and fluorescence, and (3), methods for model inversion.

2.1. Vegetation parameters, chlorophyll fluorescence and vegetation growing condition

One of the vital aspects of vegetation we are interested in is the growing condition, which includes plant structure, development, biochemistry and metabolism. Vegetation growing condition can help indicate agriculture production, carbon circulation and ecosystem function. Analysis of photosynthesis process and carbon exchanges between soil, vegetation and atmosphere can help us understand vegetation's growing condition.

2.1.1. Relation between vegetation parameters and vegetation growing condition

Vegetation parameters represent different levels of varies biophysical properties of vegetation. Common vegetation parameters include leaf area index, chlorophyll content, dry matter content, nitrogen content, leaf photosynthetic capacity and so on. Among many vegetation parameters, chlorophyll content, nitrogen and leaf area index have directly impacts on photosynthesis process (Gitelson, Peng, Arkebauer, & Schepers, 2014).

The carbon exchange between the crop canopy and the atmosphere is mainly controlled by the amount of solar radiation absorbed, the incident photosynthetic active radiation (PAR) and the fraction of PAR absorbed by photosynthetic active vegetation (fAPAR), as well as the efficiency of plants in using this energy for photosynthesis, the light use efficiency (LUE). GPP can be expressed as (J. L. Monteith, 1997):

$$GPP = PAR \times fAPAR \times LUE \qquad (2\text{-}1)$$

Chlorophylls are vital pigments for photosynthesis of plants, because the reaction centre of chlorophyll absorb light energy and transfer it to other parts of photosystem. It is found that canopy chlorophyll content is closely related to fAPAR when chlorophyll content less than 2 g m^{-2}. However GPP remains sensitive to total canopy chlorophyll even when chlorophyll content is larger than 2 g m^{-2} (Peng, Gitelson, Keydan, Rundquist, & Moses, 2011). Variations in leaf chlorophyll are well correlated with temporal changes in LUE (Houborg, Anderson, Daughtry, Kustas, & Rodell, 2011). Therefore chlorophyll content can both influence fAPAR, LUE and of course GPP though Equation 2.1. Figure 1 indicates the relation between chlorophyll multiplied by PAR and GPP.
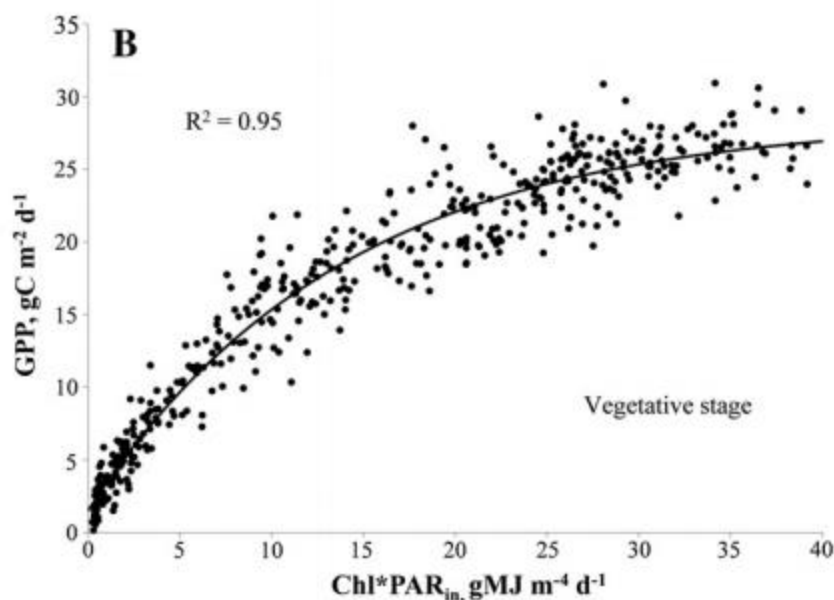
Figure 1.Relationships between GPP and Chl * PARin in rained and irrigated maize during vegetative stages from 2001 to 2010 (Gitelson et al., 2014).

Chlorophyll content also varies with the seasonal growing cycle of the plant. Figure 2 indicates the changing trend of chlorophyll content of corn and soybean from May to August in USA in 2002. In this case, chlorophyll content of soybean reached the maximum in June, while corn reached the maximum in July. There are difference in chlorophyll trend between C3 and C4 plant, but both reached maximum value of chlorophyll content in summer which have maximum temperature and rainfall. Therefore information of chlorophyll content of vegetation can be used to indicate plants' seasonal condition and other features.
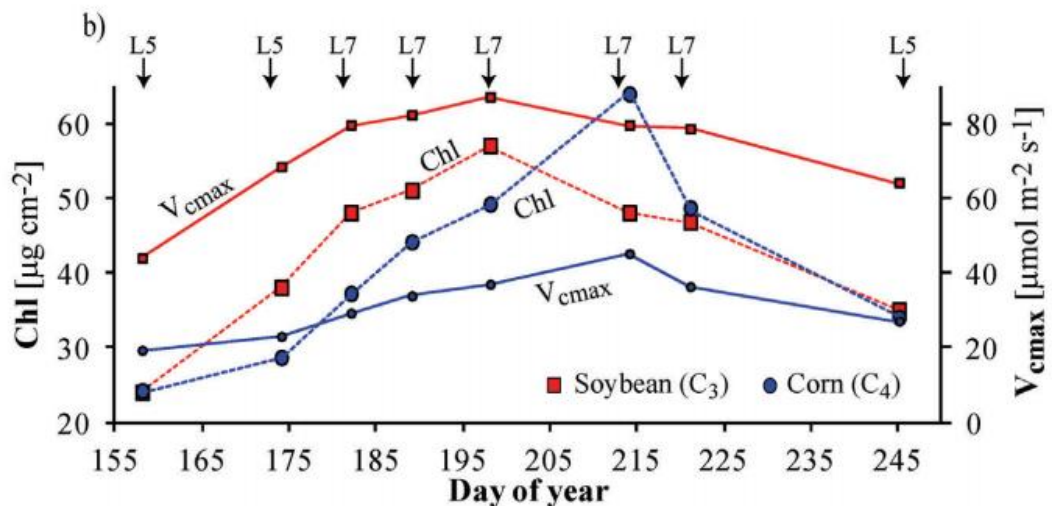
Figure 2. Time-series of satellite (Landsat 5 (L5) and Landsat 7 (L7) retrieved Chl and associated V_{cmax} for a corn and soybean field in central Iowa, U.S.A. in 2002 (Houborg et al., 2012).

Leaf Nitrogen is also vital parameter to vegetation. It was indicated that leaf nitrogen and V_{cmax} have near-linear correlation (Kattge, Knorr, Raddatz, & Wirth, 2009). V_{cmax} (maximum rate of carboxylation) governs leaf photosynthetic efficiency and defines the biochemical capacity of leaves to assimilate CO_2. This parameter plays a limiting role on actual GPP, therefore leaf nitrogen is constraint for vegetation photosynthesis process (Houborg, Cescatti, & Migliavacca, 2012). Meanwhile, chlorophyll content and nitrogen also have been proven to have strong relations (Sage & Pearcy, 1987). Therefore V_{cmax} can be acquired from chlorophyll content by relations of Chlorophyll, nitrogen and V_{cmax}.

Leaf area index (LAI) is defined as the ratio of leaf surface area to unit ground surface area (Bréda, 2003). LAI describes the available surface area for leaf gas exchange between atmosphere and terrestrial biosphere (Cowling & Field, 2003). It is an important parameter controlling many biochemical and physical processes of vegetation, including transfer of both substance and energy. LAI can be separated into photosynthetic and non-photosynthetic components. The part of LAI composed of green leaf area is called Green LAI (Viña, Gitelson, Nguy-Robertson, & Peng, 2011). Figure 3 indicates that Green LAI and GPP have obvious relations in the vegetative stage.
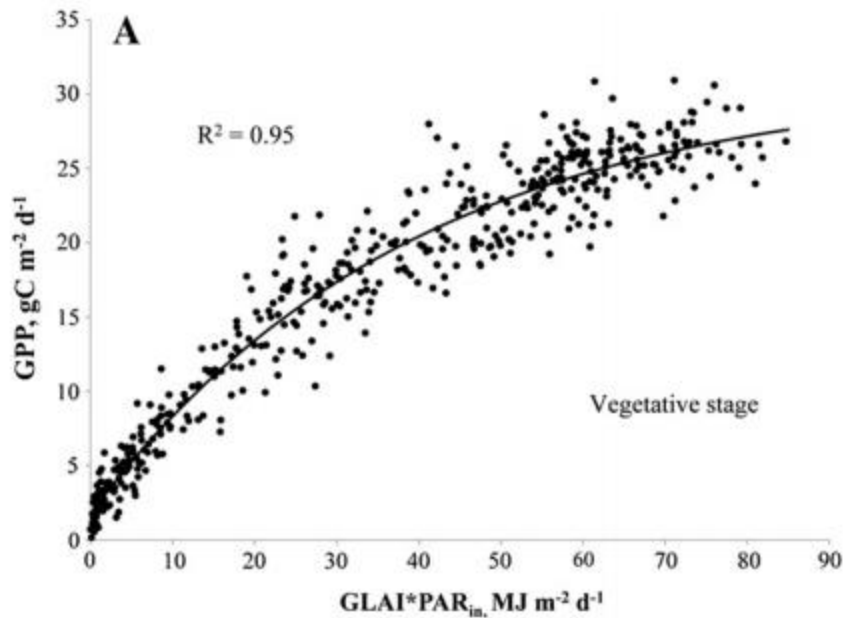
Figure 3.Relationships between GPP and GLAI ∗ PARin in rained and irrigated maize during vegetative stages from 2001 to 2010 (Gitelson et al., 2014).

2.1.2. Relation between chlorophyll fluorescence and vegetation growing condition

Chlorophyll molecules are excited when green leaves are illuminated. This excitation energy will be partly used for the process of photosynthesis while another part will be dissipated as heat and red light (chlorophyll fluorescence) (G.seaton & D.walker, 1990). Because of the relation between chlorophyll fluorescence and photosynthetic electron transport, fluorescence emissions in photosynthetic organisms could be correlated to their photosynthetic rates. Therefore chlorophyll fluorescence measurement is applied to examine photosynthetic performance and stress in algae and plants, also to identify causes of changes in photosynthesis and plant performance. It was indicated that fluorescence can be a very powerful tool to study photosynthesis performance (Baker, 2008).

However, the underlying theory of fluorescence change is complex, therefore the correct explanation for fluorescence change is difficult (Baker, 2008). According to the model for photosystem II (PSII) photochemistry (Butler, 1978), photosynthesis competes with processes of fluorescence emission and heat loss from excitation energy in the pigment antenna of PSII. Then the decline in fluorescence could both be caused by the electrons transfer from reaction center chlorophyll to PSII, and by increases in rate of heat loss. The decline of fluorescence because of increase in photosynthesis is named photochemical quenching. The decline of fluorescence because of increase in heat loss is named non-photochemical quenching (Baker, 2008). Research has indicated that there are large changes in the rate of heat loss from the antenna of PSII (Krause & Jahns, 2004). In order to estimate photosynthesis from fluorescence, it is important to distinguish and analyze fluorescence quenching which results from photochemical

quenching and non-photochemical quenching(Baker, 2008). Therefore the relation between fluorescence signal and photosynthesis is complex.
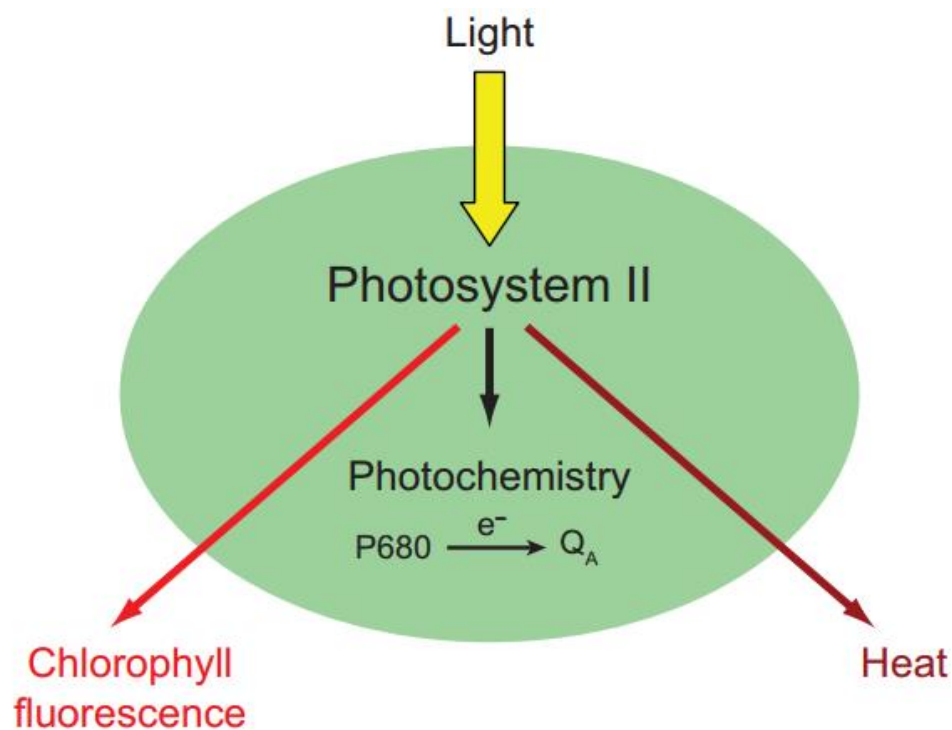
Figure 4.Simple model of the possible fate of light energy absorbed by photosystem II (PSII)(Baker, 2008).

2.2. The role of vegetation parameters on the reflectance spectrum

Different vegetation parameters like leaf area index, chlorophyll content, water content and leaf structure can represent vegetation conditions generally. Leaf and canopy conditions will change the way of absorption, scattering and transmittance of solar radiance, therefore different values and combinations of vegetation parameters can result in different reflectance (R) of solar radiance.

Radiative transfer model (RTM) includes specific mathematic equations of physical interaction processes between light, plant and soil. Among all the codes of RTM during the last recent years, the SAIL canopy reflectance model (Verhoef, 1984) and the PROSPECT leaf optical model are most popular (Stéphane Jacquemoud et al., 2009).

In PROSPECT model, scattering of light is modelled by leaf structure parameter N and spectral refractive index. Absorption is simulated by chlorophyll pigment concentration (C_{a+b}), water content (C_w) and corresponding specific spectral absorption coefficients (K_{a+b} and K_w) (S. Jacquemoud & Baret, 1990a). The coefficients K are spectra for the absorption of different constituents of the leaf. For example, chlorophyll has absorption peaks at 679nm and 703nm (le Maire, François, & Dufrêne, 2004).

The combined PROSPECT model and SAIL model is called PROSAIL model (Stéphane Jacquemoud et al., 2009). Sensitivity analyses of PROSAIL show the effects of vegetation parameters on the reflectance spectrum. Leaf chlorophyll and leaf area index were considered as the main contribution of spectral shifts in red and near-

infrared (NIR) wavelength. Leaf chlorophyll absorbs light in red wavelength, but not in the NIR. Radiation in the NIR region is mostly scattered in the vegetation. The contribution of Leaf area index LAI to reflectance spectrum is presented in Figure 5 which indicates the sensitivity of LAI from 0 (bail soil) to 10 (very dense vegetation) to reflectance spectrum. This figure shows that increase of LAI can result in decrease of reflectance in red wavelength and increase of reflectance in near-infrared. As shown in Figure 6, the average leaf angle also affects the reflectance in the NIR, and water content C_w has an average contribution of 50% to reflectance spectrum from 1450nm to 2100nm in shortwave infrared (SWIR). The effect of vegetation parameter A may depend on the value of parameter B, and therefore parameter interactions effects to reflectance spectrum have to be considered (see Figure 7). In this case, C_{ab} - LAI and C_{ab} -ALA have the contribution of each 8% to visible reflectance spectrum. LAI - ALA have 7% contribution in NIR part. In SWIR part, dominate factors depend on wavelength of reflectance spectrum.
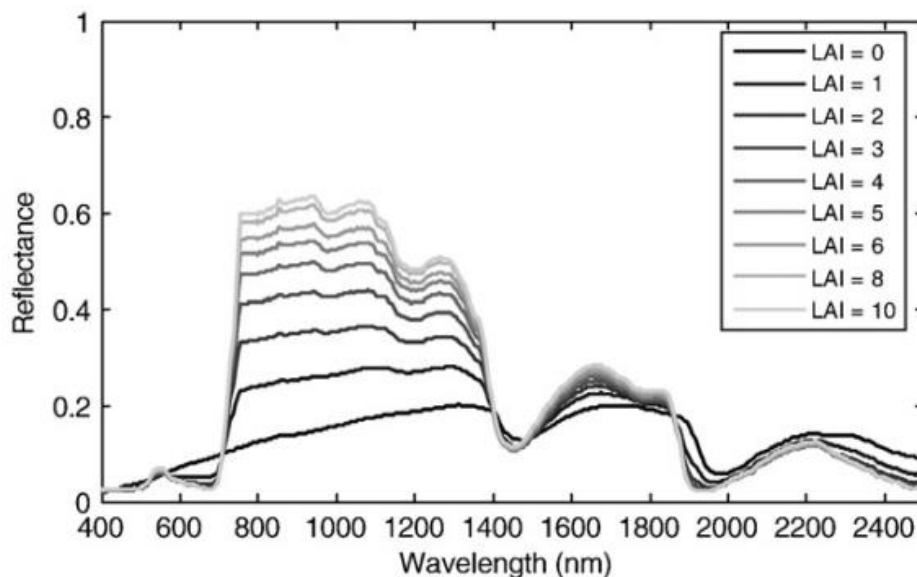
Figure 5. Effect of LAI on canopy reflectance using PROSAIL (θs=20°, θv=0°, φsv=0°, horizontal visibility=100 km, LIDF=spherical, sL=0.25, N=1.5, Cab=50 µg cm− 2, Cw=0.01 cm, and Cm=0.005 g cm−2) (Stéphane Jacquemoud et al., 2009).
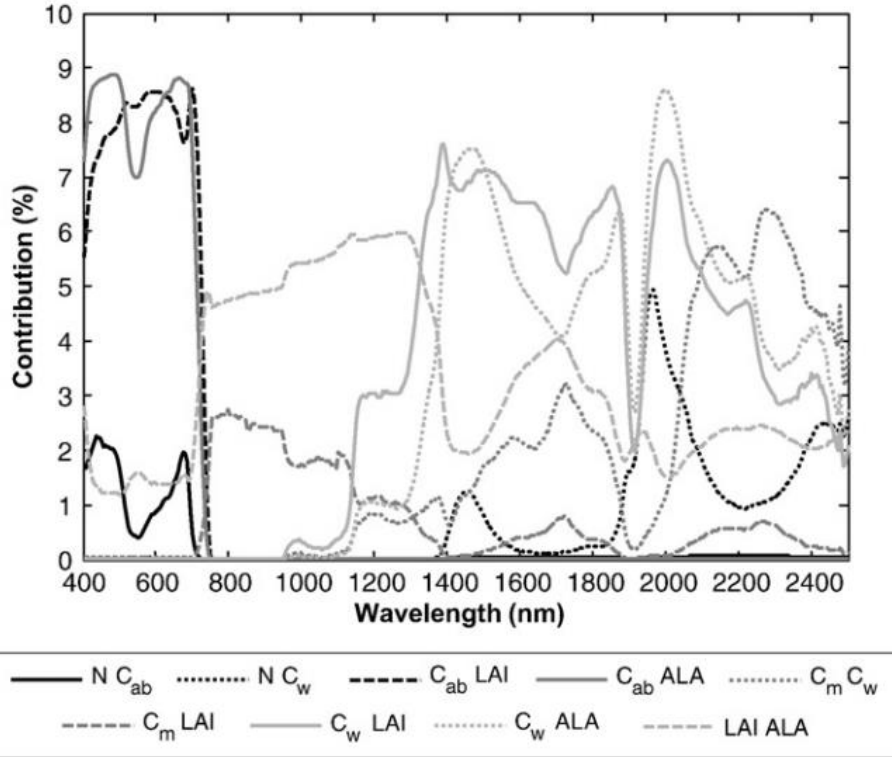
Figure 7.Spectral variation of the contributions of interactions of the PROSAIL variables to the top-of canopy reflectance. Solar zenith angle θs=31.6° (Stéphane Jacquemoud et al., 2009).
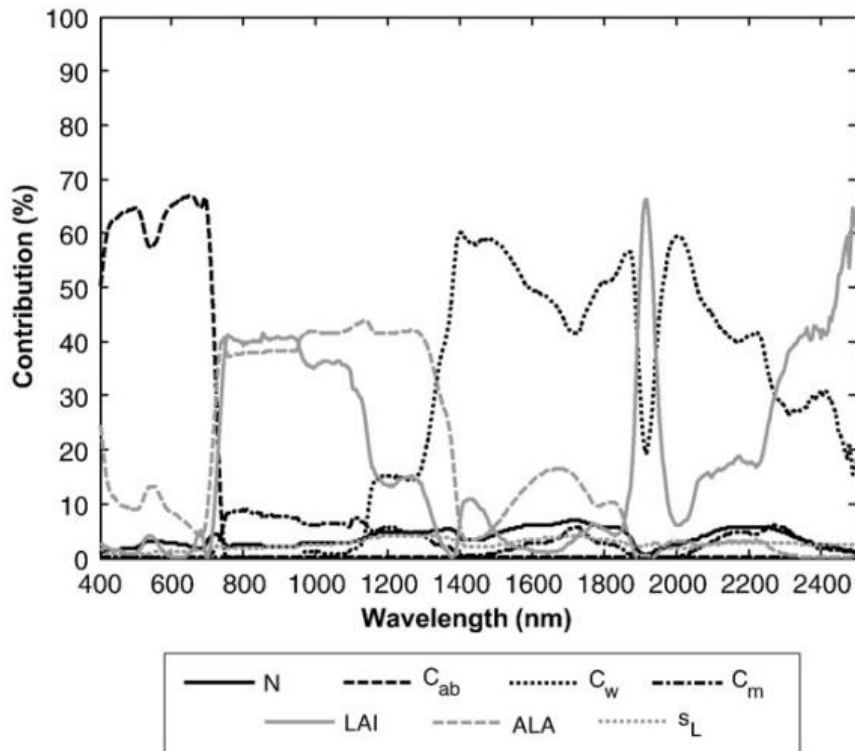
Figure 6.Spectral variation of the contributions of the PROSAIL variables to the top-of canopy reflectance. Solar zenith angle θs=31.6° (Stéphane Jacquemoud et al., 2009).

2.3. The role of vegetation parameters on chlorophyll fluorescence

Although there is little literature about relations between vegetation parameters and chlorophyll fluorescence, physical theories which include relations between vegetation parameters and chlorophyll fluorescence are already used to simulate plant fluorescence. There are a few models that describe the relations between parameters and fluorescence, at leaf level and at canopy level.

For simulation of leaf fluorescence, FluorMODleaf (Pedrós, Goulas, Jacquemoud, Louis, & Moya, 2010) which is a model of chlorophyll fluorescence was built based on PROSPECT model. Number of elementary plates N, the total chlorophyll content C_{ab}, the total carotenoid content C_{cx}, the equivalent water thickness C_w, the dry matter content C_m, the σII/σI ratio and the fluorescence efficiency of PSI and PSII are as input data for modelling fluorescence. Relations between those parameters and fluorescence can be analyzed in Figure 8. Moreover, scattering will lengthen the optical pathway inside the leaf, causing an increase in the reabsorption in red. Relations between parameters and fluorescence are proved to be different when scattering happens (Pedrós et al., 2010).
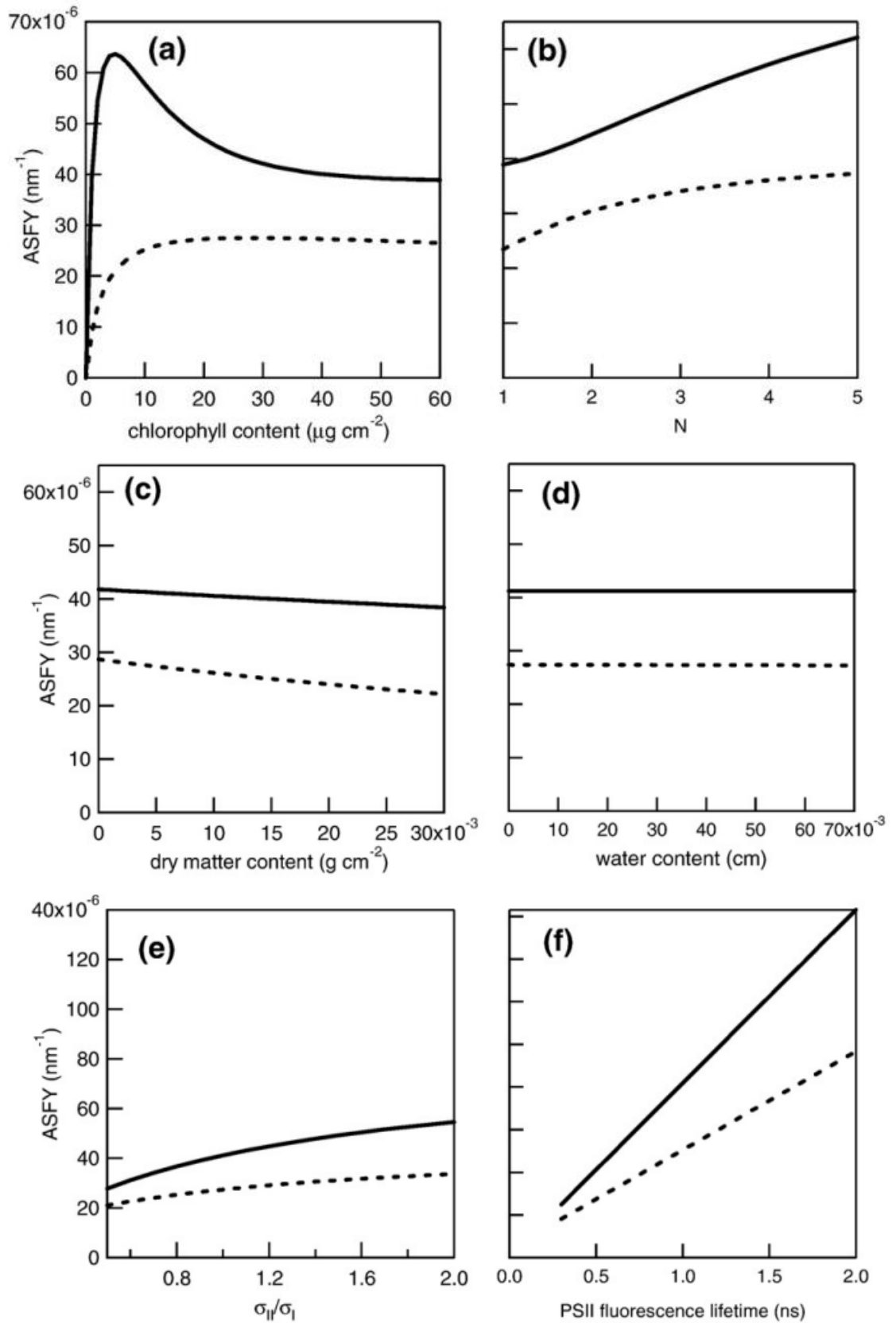
Figure 8. Apparent spectral fluorescence yield (ASFY) computed by FluorMODleaf as a function of (a) chlorophyll a+b content, (b) leaf structure parameter, (c) dry matter content, (d) water content, (e) σII/σI ratio, and (f) PSII lifetime. Solid line: emission at 685 nm, dashed line: emission at 735 nm. (Pedrós et al., 2010).

For simulations of canopy fluorescence, a recent version of the SCOPE model (van der Tol, Verhoef, Timmermans, Verhoef, & Su, 2009) which includes novel leaf physiological modules for modelling steady state fluorescence yield, has been used to analyze driving factors to canopy leaving sun-induced fluorescence (Verrelst, Rivera, et al., 2015). The results indicate that canopy SIF is driven largely by leaf chlorophyll content, vegetation structure, leaf area index and LIDFa, these four parameters can explain over 67% of the variability of the PAR part in SIF when considering only vegetation parameters. V_{cmo}, leaf photosynthetic capacity, explained for most up to 22.5% of the variability of the SIF emission efficiency part in SIF at 676 nm. In addition, micrometeorological variables also drive simulated SIF (Verrelst, Rivera, et al., 2015).

Airborne based imaging spectrometers can observe SIF data in intermediate spatial resolution. HYPLANT (Rascher et al., 2015) was specifically designed to detect vegetation and retrieve fluorescence. Data in HYPLANT consists of surface radiance from 380 to 2500 nm of spectrum, and surface radiance in the red and far-red spectrum with spectral resolution of 0.25 nm. These two data types can provide reflectance from 380 to 2500 nm, and chlorophyll fluorescence at 680 and 760 nm. (Rascher et al., 2015).

In order to obtain vegetation parameters from reflectance and chlorophyll fluorescence from remote sensing data like HYPLANT, model inversion technique is needed to inverse the forward model.

2.4.   Mathematic methods of inversion

There are different methods to establish the relation between vegetation properties and optical remote sensing. These methods include parametric regression, non-parametric regression and physically based models (Verrelst, Camps-Valls, et al., 2015). The techniques to invert remote sensing signals to obtain bio-physical parameters of vegetation are different accordingly.

For the parametric method, because the forward relation is explicit, the inversion process is simple and easily calculated by directly rearranging the equations.

For the non-parametric regression method, a learning phase based on training data is established instead of using an explicit relation. Thus the inversion techniques are more complex than for the parametric method. Decision tree learning and artificial neural networks (ANNs) are representative inversion methods. Decision tree learning is based on hierarchical connected nodes, and this method is more applied in classification than regression inversion. Random forest approach is a representative one of decision tree learning method (Mutanga, Adam, & Cho, 2012). Due to the complexity of artificial neural networks with layered structure of artificial neutrons, the performance of this method relies on its design. Too many or few of the layers and neutrons will reduce the accuracy (Mutanga et al., 2012).

For physically based method like RTM which has physical theory basis and mathematic relations, inversion techniques are also complex because of numerous unknown variables. This feature of the model may cause multiple solutions of the RTM inversion, which is called equifinality. Methods to do model inversion process include lookup table inversion, trust region optimization inversion and machine learning inversion. Lookup table method do inversion by comparing measured reflectance data with a table of model results. This table contains parameters and corresponding simulated reflectance. By looking for matching spectra one can obtain suitable vegetation parameter combinations. Trust region optimization method calculate vegetation parameters by iterations to look for satisfying minimum objective function value. Machine learning method do inversion process by seeking linear or nonlinear regression algorithms in semiautomatic and systematic manner (Caicedo, Verrelst, Munoz-Mari, Moreno, & Camps-Valls, 2014). Pros and cons of those inversion methods are listed in Table 1.

Table 1.Pros and cons of three different inversion methods.

Methods name	pros	cons
Lookup table method	Simple logic and short calculation times	Inaccurate relatively; may have different parameter combinations for same accuracy
Trust region optimization method	Relatively accurate	Time consuming for calculation; hard to operate with high-spatial resolution image in large area
Machine learning method	Accurate, robust (Caicedo et al., 2014)	Difficult to determine which regression algorithm to use

3.   STUDY SITE, DATA AND MODEL

3.1.   Study area

Study area is within Rur catchment in North Rhine-Westphalia, west of Germany, which dominated by agricultural land cover. Rur River originates from Belgium and then flows through Germany and Netherlands, and the majority parts of Rur River are in Germany. The study area is near the village of Selhausen (50°52'12.82''N, 6°26'59.59''E). Crops in this area consist of sugar beet primarily, and also include potato and corn in few places. Other land covers in this area include trees, grass, soil and urban land use.
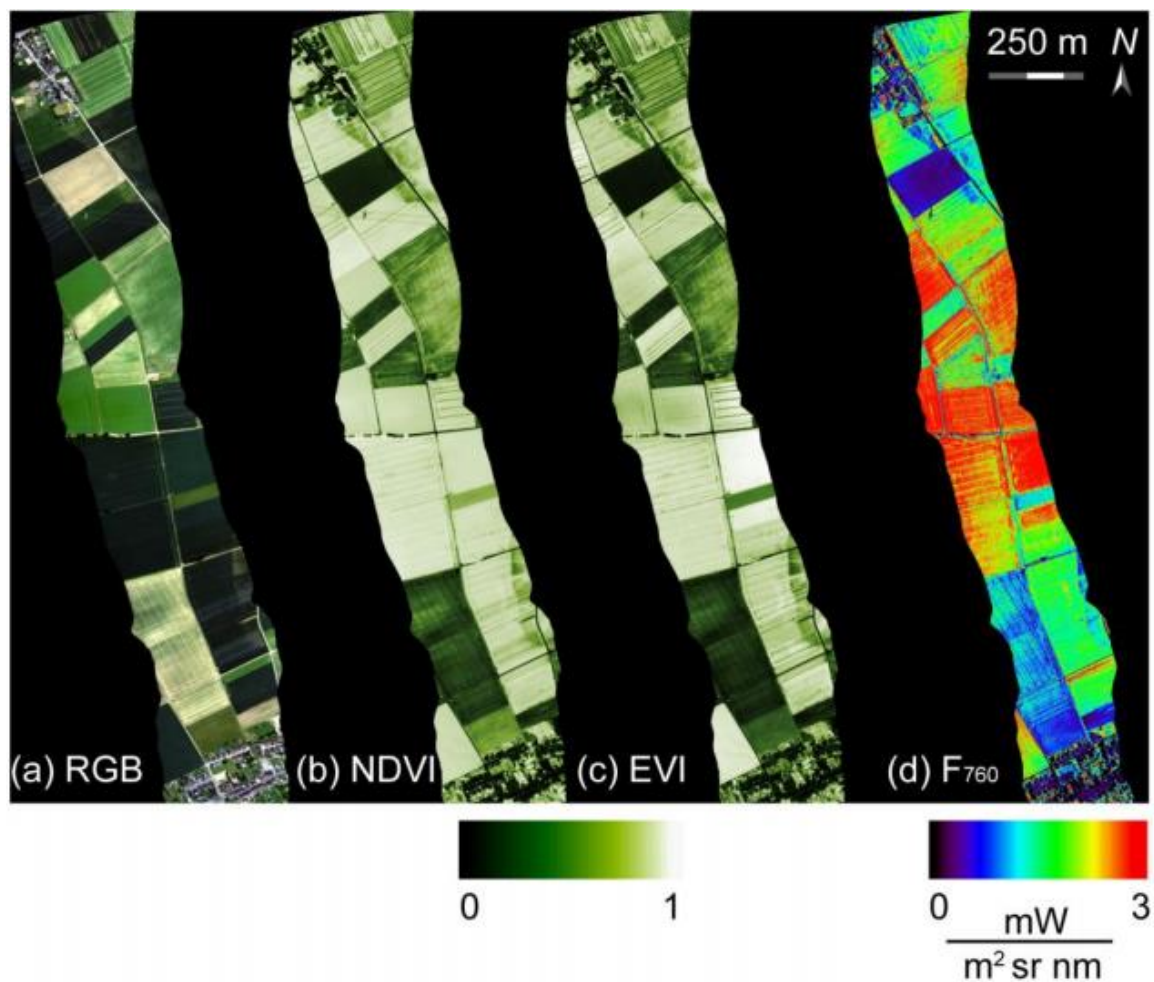
Figure 9. Study area representation with HYPLANT data. (a) Color composition in RGB of study area from airborne sensor measurements data near Selhausen. (b) Normalized Difference Vegetation Index (NDVI). (c) Enhanced Vegetation Index (EVI). (d) Fluorescence map at 760 nm. (Rascher et al., 2015)

The recent research shows that maps of SIF indicate a large spatial variability between different vegetation types (Rascher et al., 2015), therefore different vegetation types of SIF data will be modeled. Because of time consuming problems in calculation of inversion processes, limited number of pixels are chosen in different land covers types in this research. Land cover types which are considered in this research are sugar beet, corn, potato, grass and trees.

3.2. Reflectance data

Reflectance data which are used in this study are remote sensing data from airborne based imaging spectrometer HYPLANT in Germany. Specific information are in Table 2. Figure 10 shows reflectance spectrum of various vegetation types.

Table 2. Information of reflectance data from HYPLANT in this study

	Reflectance data from HYPLANT in this study
Date of data	23/08/2012
Local time	13:51 ~ 13:53
Wavelength extent (nm)	372 ~ 2484 nm
Spatial resolution	1m
Solar zenith angle (degree)	39.4
location	Selhausen, Germany
bands	622
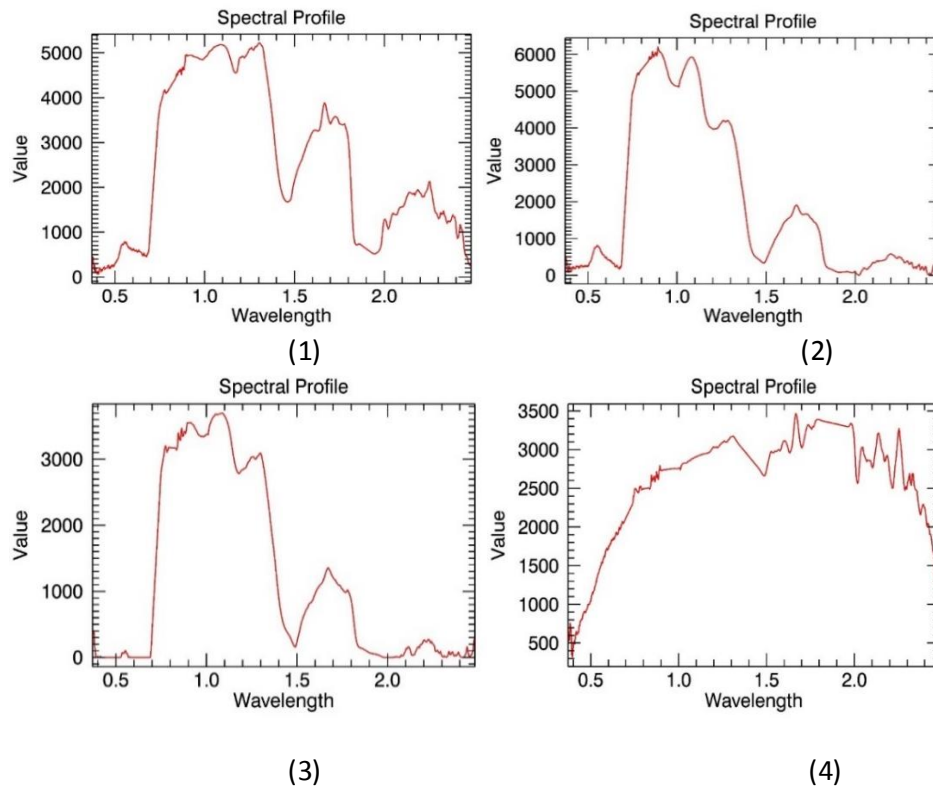
Figure 10. Representative Spectrum of grass (1), sugar beet (2), tree (3) and soil (4) (unit: fraction*10000)

3.3.   SIF data

Solar induced fluorescence (SIF) data in this study are also from HYPLANT data in the same location as reflectance data. Because of technical limits in SIF retrieval methods, only SIF data at 680 nm and 760 nm are produced in HYPLANT SIF data. SIF data of 3 flight times at same day were used. Specific information is shown in Table 3.

Table 3. Information of SIF data from HYPLANT in this study.

	Reflectance data from HYPLANT in this study
Date of data	23/08/2012
Local time	11:56, 13:50, 16:05
Wavelength extent (nm)	680 nm; 760 nm
Spatial resolution	1m
location	Selhausen, Germany
bands	2

3.4. Meteorology data

Meteorology data in this study are from flux tower in Selhausen, Germany in the same date as SIF data. Meteorology data include broadband incoming short wave radiation (W/m^2), broadband incoming longwave radiation (W/m^2), air temperature (Celcius), air pressure (hPa), atmosphere vapour pressure (hPa) and wind speed at height Z (m/s). Geographic coordinates of flux tower is 50.8658339 N / 6.4473888 E.

3.5. Models

3.5.1. RTM model in SCOPE and inversion

RTM (Radiative Transfer Model) describe the path of radiation in a medium of air, water, vegetation and urban areas.

SCOPE model is a radiative transfer and energy balance model which simulate spectral radiation and energy balance of a vegetated surface at the level of single leaves as well as at canopy level (van der Tol et al., 2009). SCOPE model has been through a period to develop its structure and components. The part to simulate interaction between radiation and plant leaves comes from Fluspect model, which is based on the PROSPECT model. PROSPECT is a radiative transfer model which describe leaf optical properties from 400 nm to 2500 nm with a minimum number of parameters in order to facilitate its inversion. Parameters include leaf mesophyll structure (N), pigment concentration, water content (C_w) (S. Jacquemoud & Baret, 1990b). Simulation of Interaction between incident light and vegetation canopies in SCOPE comes from SAIL (Scattering by arbitrarily inclined leaves) model. Extinction and scattering coefficients of a layer are calculated on the basis of a given leaf area index and a leaf inclination distribution in SAIL model (Verhoef, 1984).

After the forward model from vegetation parameters to reflectance, the inversion of RTM model is required to convert reflectance to vegetation parameters

A newly developed code to tune the SAIL model to reflectance in MATLAB are used to do RTM model inversion to get vegetation parameters. After iterating and minimizing differences between modeled reflectance with measured reflectance, vegetation parameters are obtained. This method belongs to the trust region optimization method which is time consuming, therefore this method cannot be applied to the whole image.

3.5.2. SVAT model in SCOPE

SVAT (Soil-Vegetation-Atmosphere-Transfer model) describes the transport processes of energy, momentum, wind, and mass of water, carbon, nutrients (Van Der Tol, Rossini, Rascher, Verhoef, & Mohammed, 2016). SCOPE model obtain reflectance and fluorescence in the observation direction as a function of the solar zenith angle and leaf inclination distribution (Verrelst, Rivera, et al., 2015). In SCOPE model, after the absorbed radiation within canopy is calculated, the distribution of absorbed radiation is further used in a micrometeorological model of the canopy for the calculation of photosynthesis, fluorescence, latent and sensible heat. The fluorescence and thermal radiation emitted by individual leaves is finally propagated through the canopy (van der Tol et al., 2009). Fluspect was included to simulate SIF of the leaf. SIF can be modelled from vegetation parameters which include leaf parameters and canopy parameters. In addition, meteorology data are also needed here because parameters like air temperature and air pressure are considered to have effects on SIF.
Vegetation parameters which will be used are as below:

Chlorophyll content (Cab);
Dry matter content (Cdm);
Leaf water thickness equivalent (Cw);
Senescent material (Cs);
Leaf area index (LAI);
Leaf inclination (LIDF);
Leaf structure parameter (N);

3.5.3. GSV model

A separate model was used for the soil reflectance, notably the GSV (global soil vectors) (Jiang & Hongliang, 2012) model. GSV model can represent any dry soil spectrum with soil spectral vectors and 3 coefficients as equation below.

$$S' = G \times a \qquad (3\text{-}1)$$

Where S' means the spectrum which are needed; G means soil spectral vectors; a means 3 coefficients.

To get coefficients 'a', one way is to do with matrix calculation. Given soil spectrum need to be transformed and equation below are used (Verhoef, Tol, & Middleton, 2014)

$$a = (G^T G)^{-1} G^T S \qquad (3\text{-}2)$$

Where $\mathbf{G^T}$ means transformed G; G means soil spectral vectors; a means 3 coefficients, s means given soil spectrum.

4.   METHOD

Introduction

In this chapter, the methods which were performed during this research will be explained in detail. A flow chart is presented below in Figure 2.

Chapter 3.1 explains the dataset selection criteria and dataset structure which were used in research.

Chapter 3.2 discusses operation process of inversion with RTM model. Input data preparation, initial value select and parameters retrieval will be explained respectively.

Chapter 3.3 explains process details of SIF simulation with the SCOPE (FLUSPECT) model.
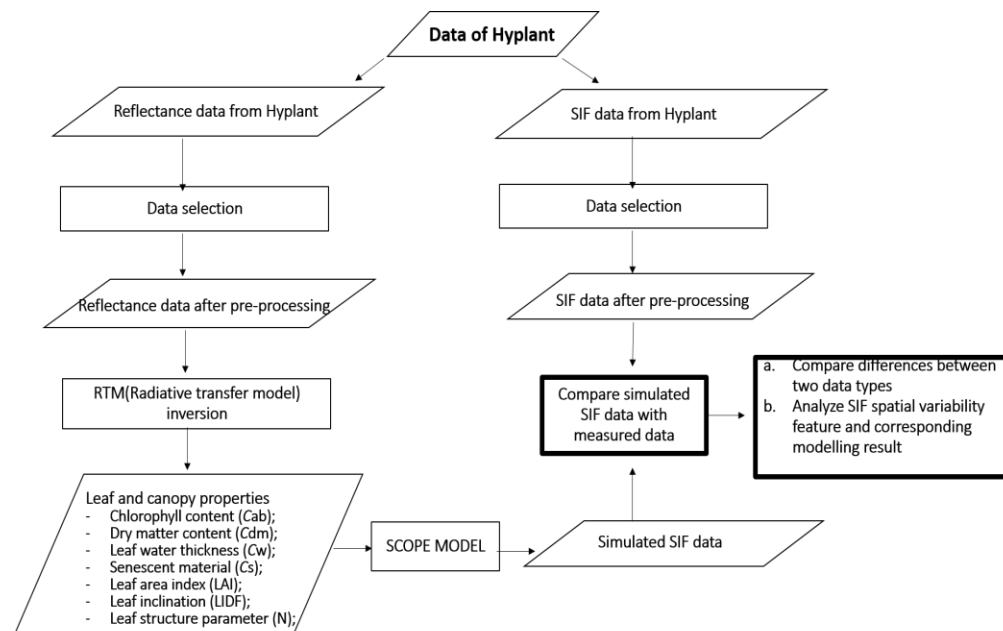
Figure 11 .Flowchart about methods to be used in this research.

4.1.   Dataset selection

Airborne measured surface reflectance data and SIF data were used as data source to perform SIF variability analysis, SIF simulation and SIF comparison. Both reflectance and SIF datasets are airborne remote sensing image, therefore both of them have spatial distribution features. To Represent SIF variability needs relatively large amount of pixel samples. Because SIF modelling process is time consuming, it is not possible to simulate and compare too many pixels in the image. Then the datasets should be both operable in analysis process and representative in image spatial features. So the design of datasets are key part of data processing.

According to feature of data spatial variability, two type of datasets are classified: representing different land covers, representing variability of SIF in transient area inside one land cover. Then for each of them, two subclasses are chosen: one relatively small area for modelling and comparison, one relatively large area for SIF variability analysis.

4.1.1. Dataset 1: representing typical different land covers

In extent of the data image, five plant species have been classified, notably sugar beet, corn, grass, potato and trees. Thus datasets should include the pixels which contain representative features of these plant species. These pixel samples should not be influenced by surrounding factors like road or cable (adjacency effect).

In Subclass 1, 6 pixels per vegetation type are used to represent one plant species. This subclass data are used to SIF simulation and SIF comparison for different vegetation type.

In Subclass 2, corn, tree, grass, sugar beet and potato have 418 pixels, 240 pixels, 504 pixels, 672 pixels and 192 pixels respectively. This subclass data are used to analyze variability of SIF for different land cover.

4.1.2. Dataset 2: representing areas inside one land cover which have obvious SIF variability of HYPLANT SIF data

Because of obvious variability of SIF inside one plant species, it is necessary to choose representative SIF value changing area of same plant species and to check if model can simulate these relatively large changes. Because sugar beet have large cover area in the study area compared to other vegetation types, therefore SIF changing data in sugar beet has been used as example of transient phenomena.

In Subclass 1, small area which include 18 pixels with obvious changing SIF inside sugar beet field were chosen. SIF simulation and SIF comparison were made with this subclass data for transient area.

In Subclass 2, relatively large area with 348 pixels with obvious changing SIF inside sugar beet field were chosen. Variability of SIF were analyzed with this data for transient area.

The locations of chosen area are approximately represented in Figure 12 and Figure 13.
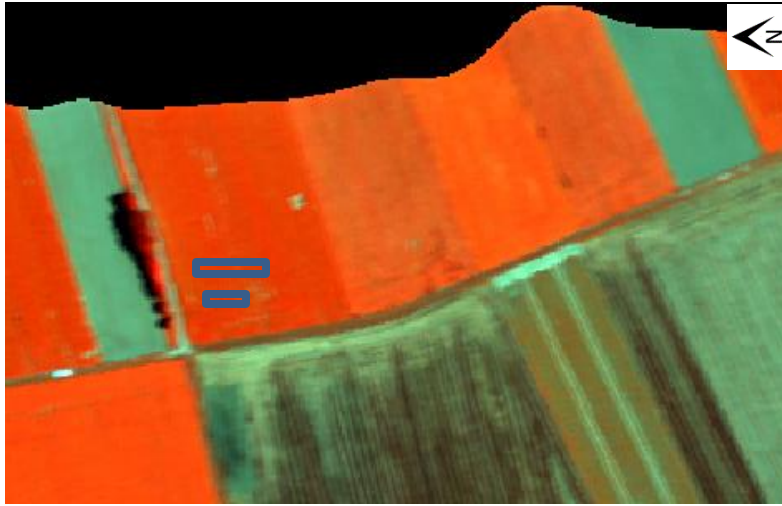
Figure 12.Data location and RGB image of reflectance data in study area: R 859nm, G 550nm, B 459 nm.
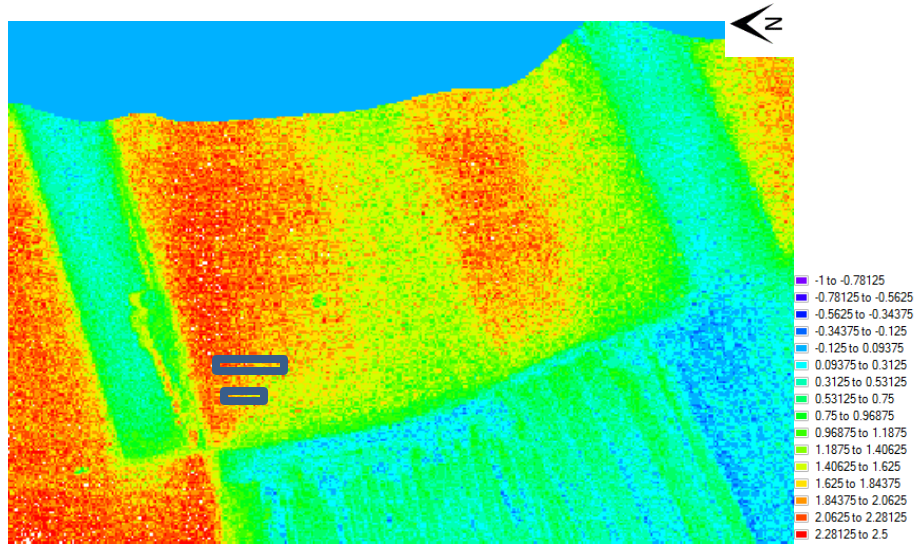
Figure 13.Data location and SIF at 760 nm of study area.

4.2. Simulation with RTM model

4.2.1. Input data preparation

After data selection, geographical locations and coordinates of these chosen pixels have been recorded. Canopy reflectance spectrum data of each pixel in 622 bands from 371.84 nm to 2483.4 nm were been taken. In ENVI 5.1 version, image data can be saved as an ASCII file containing digital information for each line, row and band in image. These arrays with digital number can be processed in MATLAB. A simple code in MATLAB was used to convert 3 dimensional array to 2 dimensional array. After using this function, the original array of reflectance data can be processed and saved as expected format (.dat) in ASCII. Those reflectance data were supposed to be used as main source of input data for RTM model.

Another type of input data for model is soil spectrum. In order to have more reliable results, a local soil spectrum was preferred instead of model default soil spectrum data. In this case, the local soil spectrum was chosen from bare soil reflectance data of the

same HYPLANT reflectance image as previous step. According to input data requirements to soil spectrum in RTM model inversion, soil spectrum as input data should have integer wavelength expressed in nanometers. Because HYPLANT reflectance measurement data's wavelength were non-integer, it was necessary to resample the soil reflectance with the function 'interp1' in MATLAB. The code 'YI = INTERP1(X, Y, XI, METHOD)' interpolates to find YI, the values of the underlying function Y at the points in the array XI (MATLAB 7.12.0 product help). So X and Y were replaced by original wavelength and original reflectance, and XI and YI were replaced by new integer wavelength and new reflectance here.

After this, the local soil spectrum still had some noise, so a smoothing operation was required. The GSV (global soil vectors) (Jiang & Hongliang, 2012) model uses 3 basic soil vector components to fit any given dry soil reflectance spectrum. The equation is as follow:

$$S = a_1 g_1 + a_2 g_2 + a_3 g_3 \tag{4-1}$$

Where g_1, g_2, g_3 are 3 basic soil vector, and a_1, a_2, a_3 are 3 coefficients to approximate a given soil spectrum. S is modelled soil reflectance with least squared error statistical approach.

'Solver' function in EXCEL was used to find the proper a_1, a_2, a_3 to make squared error of differences between original soil reflectance and modelled soil reflectance minimum. By calculating a_1, a_2, a_3, local soil spectrum with smooth curve was obtained.

4.2.2. Initial value of vegetation parameters

In order to have more reliable model results, vegetation parameters initial values' effects to model results were examined. Vegetation parameters in this model include Chlorophyll content (C_{ab}), Dry matter content (C_{dm}), Leaf water thickness equivalent (C_w), Senescent material (C_s), Leaf area index (*LAI*), Leaf inclination (*LIDF*), Leaf structure parameter (*N*).

Ideally the retrieval does not rely on the initial values of vegetation parameters. To test whether this was the case, the retrieval results were been checked when vegetation parameters have different initial values. First each vegetation parameter's initial value was changed individually to see the variations of model result. Then all vegetation parameters' initial values were changed together to see the variations of model result. If the result maintain nearly the same in both changing approach, then the choice of initial values is not important for the result. If result change obviously, then the choice of initial values should be made carefully.

4.2.3. Vegetation parameters' retrieval

After preparation of input data and observation of vegetation parameters' initial value's effect on the model result, parameters can be retrieved by RTM model. The model was set up such that the following parameters were tuned: C_{ab}, C_{dm}, C_w, C_s, *LAI, LIDF* and C_{ca}. The parameter *N* with its initial value of '5' was not tuned.

4.3. Fluorescence simulation

After getting vegetation parameters to describe plant condition, SIF spectrum from 640 nm to 850 nm can be modelled in SCOPE with meteorological data from the weather station (the eddy covariance tower).

Firstly filenames and locations of output file were defined. Secondly each parameters' value (Cab, Cdm, Cw, Cs, LAI, LIDFa, LIDFb, N and Cca) needs to be defined, and these values come from the RTM model inversion results described in Section 4.2. The third part to be defined is the weather conditions, which include broadband incoming shortwave radiation (W m^{-2}), broadband incoming longwave radiation (W m^{-2}), air temperature (Celcius), air pressure (hPa), atmospheric vapour pressure (hPa), wind speed at height z (m s^{-1}). These meteorology data come from flux tower logger in study area. Also time of measurement should fit the airborne flight time of HYPLANT data, which is used to calculate the solar angle. Carboxylation capacity V_{cmo} was kept at default values, because there are no measurements for this parameter.

5. RESULTS

5.1. Result of simulation and comparison for different landcovers

5.1.1. Vegetation parameters

Vegetation parameters from different land covers (sugar beet, grass, tree, corn and potato) have been retrieved for 6 pixels per cover type. Representative vegetation parameters which are average value of 6 pixels per land cover are in Table 4. Corn had highest C_{ab} of 65.36 ug cm^{-2}, while grass had the lowest C_{ab} of 17.32 ug cm^{-2}. Corn had highest C_w of 0.036 mg cm^{-2}, and grass had lowest C_w of 0.007 mg cm^{-2}. Trees had highest C_{dm} of 0.0056 mg cm^{-2}, and sugar beet had lowest C_{dm}. Grass had highest C_s of 0.39, and corn had lowest C_s of 0.11. Tree had highest C_{ca} of 21.80 ug cm^{-2}, and potato had lowest C_{ca} of 7.32 ug cm^{-2}. Corn had highest LAI of 4.70, and potato had lowest LAI of 1.79. Sugar beet had highest LIDFa of 0.589, and corn had lowest LIDFa of -0.136.

Table 4.Modelled representative vegetation parameters of sugar beet, corn, grass, potato and tree. (RMSE: root mean square error)

Parameters	Sugar beet	Corn	Grass	Potato	Tree
C_{ab} (ug cm-^{2})	26.23	65.36	17.32	21.96	60.15
C_w (mg cm^{-2})	0.035	0.036	0.007	0.021	0.031
C_{dm} (mg cm^{-2})	2.22E-14	0.0042	0.0022	1.19E-08	0.0056
C_s (fraction)	0.13	0.11	0.39	0.19	0.14
C_{ca} (ug cm^{-2})	7.68	20.39	7.77	7.32	21.80
N (dimensionless)	1.5	1.5	1.5	1.5	1.5

LAI	3.32	4.70	3.26	1.79	4.22
LIDFa	0.589	-0.136	-0.035	0.211	0.030
LIDFb	-0.12	-0.57	-0.67	-0.45	-0.62
RMSE (mod-meas spectra)	0.015	0.017	0.029	0.020	0.021

5.1.2.   Modelled SIF spectrum and comparison at noon

After having vegetation parameters of different vegetation covers and weather data from flux tower, SIF spectrum of different vegetation types can be modelled from SCOPE model for 6 pixel samples per vegetation type. Results were presented in Figure 14.
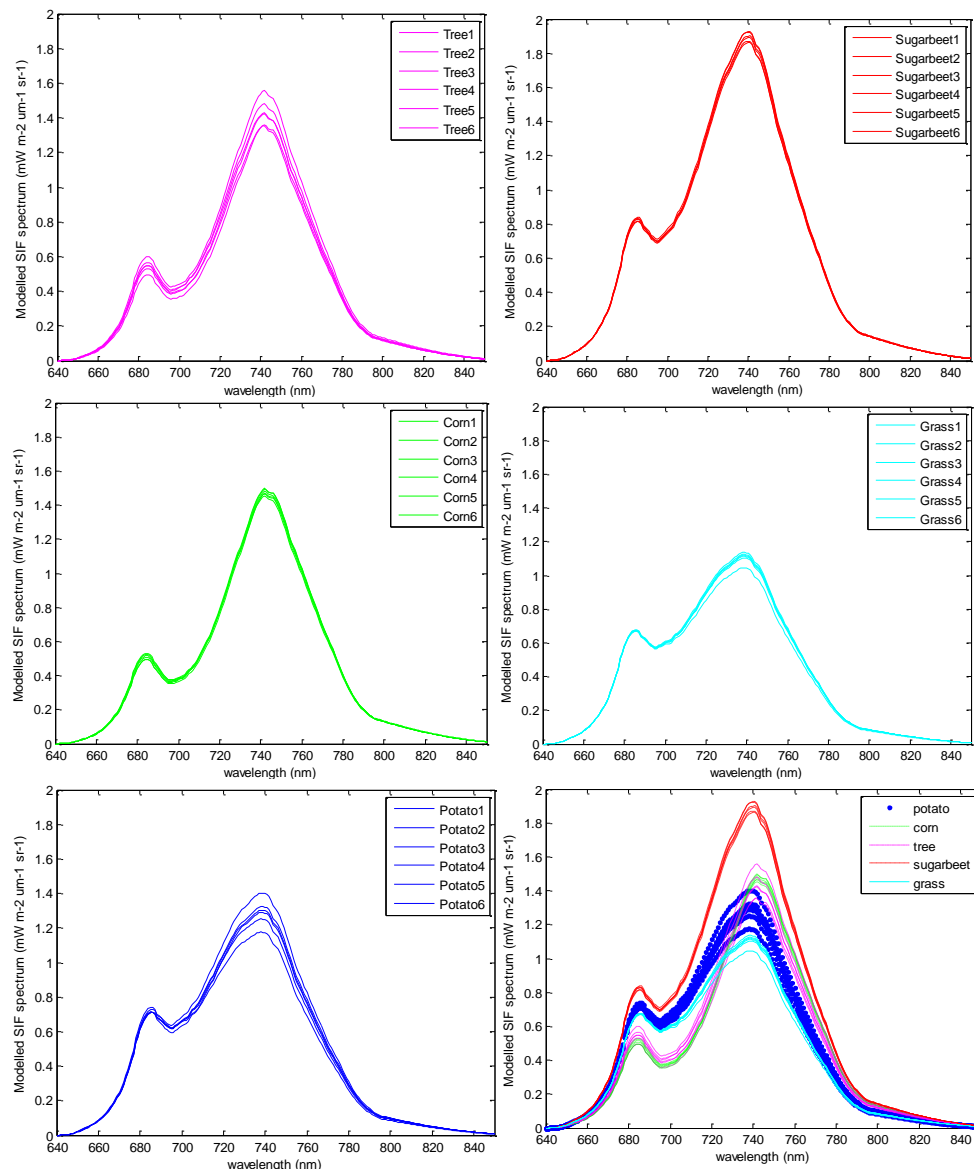

Figure 14.SIF simulation of Tree, Sugar beet, Corn, Grass, Potato and from SCOPE model.

For SIF at 680 nm, SIF value from highest to lowest are sugar beet, potato, grass, tree and corn. For SIF at 760 nm, SIF value from highest to lowest are sugar beet, corn,

tree, potato and grass. Tree and potato have relatively large variability in modelled SIF spectrum between each pixel, while corn, sugar beet and grass have relatively small variability in modelled SIF spectrum between each pixel.

Comparison between measured and modelled SIF data can be made at 680 nm and 760 nm. Figures below compare modelled and airborne measurement SIF data of five vegetation types at two wavelength respectively.
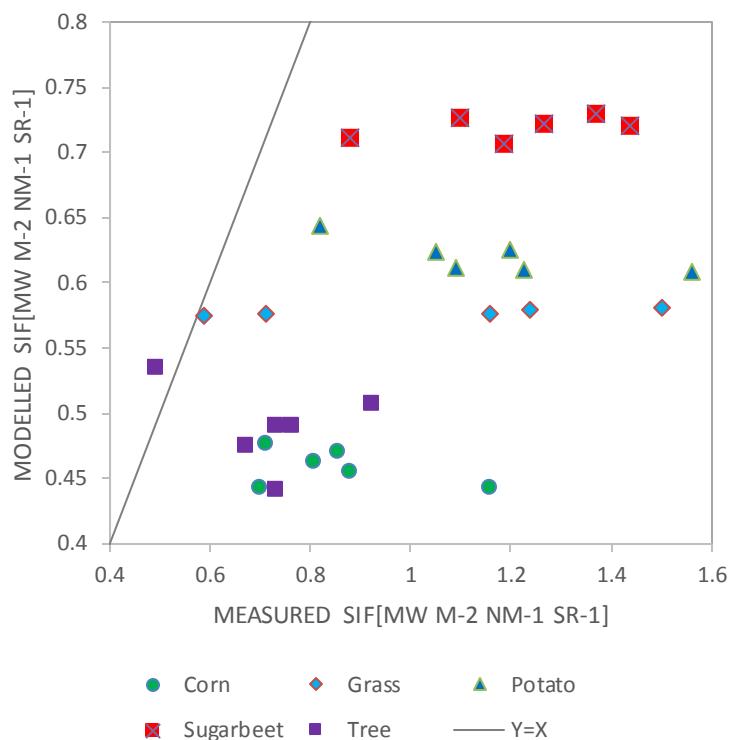

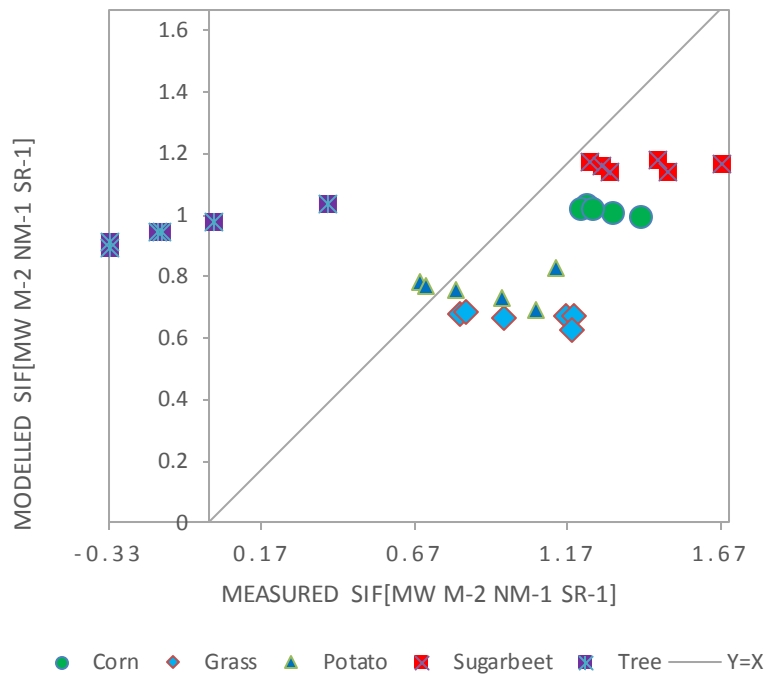Figure 15.Comparison between measured SIF data by HYPLANT and modelled SIF data at 680 nm.

Figure 16.Comparison between measured SIF data by HYPLANT and modelled SIF data at 760 nm.

For comparison at 680 nm in Figure 15, measurements data of sugar beet are from 0.85 to 1.45 mW m^{-2} um^{-1} sr^{-1}, while most modelled result of sugar beet are near 0.7 W m^{-2} um^{-1} sr^{-1}. Measurements data of potato are from 0.8 to 1.6 W m^{-2} um^{-1} sr^{-1}, while modelled SIF of potato are near 0.65 W m^{-2} um^{-1} sr^{-1}. Measurements data of grass are from 0.55 to 1.5 W m^{-2} um^{-1} sr^{-1}, while modelled SIF of grass are near 0.6 W m^{-2} um^{-1} sr^{-1}. Measurements data of tree are from 0.45 to 0.9 W m^{-2} um^{-1} sr^{-1}, while modelled SIF of tree are near 0.45 W m^{-2} um^{-1} sr^{-1}. Measurements data of corn are from 0.7 to 1.15, while modelled SIF of corn are near 0.45 W m^{-2} um^{-1} sr^{-1}. Variations of measured SIF are wider than modelled SIF.

In comparison at 760 nm in Figure 16, results plot at 760 nm have more obvious patterns to distinguish different vegetation types than at 680 nm. However, the variations of measured SIF are also wider than modelled SIF. Measurements data of sugar beet are from 1.17 to 1.67 W m^{-2} um^{-1} sr^{-1}, while most modelled result of sugar beet are near 1.2 W m^{-2} um^{-1} sr^{-1}. Measurements data of potato are from 0.67 to 1.17 W m^{-2} um^{-1} sr^{-1}, while modelled SIF of potato are near 0.75 W m^{-2} um^{-1} sr^{-1}. Measurements data of grass are from 0.7 to 1.2 W m^{-2} um^{-1} sr^{-1}, while modelled SIF of grass are near 0.75 W m^{-2} um^{-1} sr^{-1}. Measurements data of tree are from -0.3 to 0.47 W m^{-2} um^{-1} sr^{-1}, while modelled SIF of tree are near 1 W m^{-2} um^{-1} sr^{-1}. Measurements data of corn are from 1.17 to 1.47, while modelled SIF of corn are near 1.2 W m^{-2} um^{-1} sr^{-1}.

For both wavelength and all vegetation types, variations of modelled SIF are smaller than measured SIF.

5.1.3. Modelled SIF spectrum and comparison at multi-time in one day

SIF of different land covers at different time (local time: 11:56, 13:50, and 16:05) have been modelled. Figure 17 are the results of modelled SIF spectrum of different land covers. It shows that at time 2 (13:50), SIF values are highest, and at time3 (16:05) SIF values are lowest for all land cover types. The reason could be the differences of short wave irradiance for different local times.

The high irradiance at 13:50 result in relatively high SIF at two peaks, while the low irradiance at 16:05 result in relatively low SIF at two peaks.

(a)

(b)

(c)

(d)
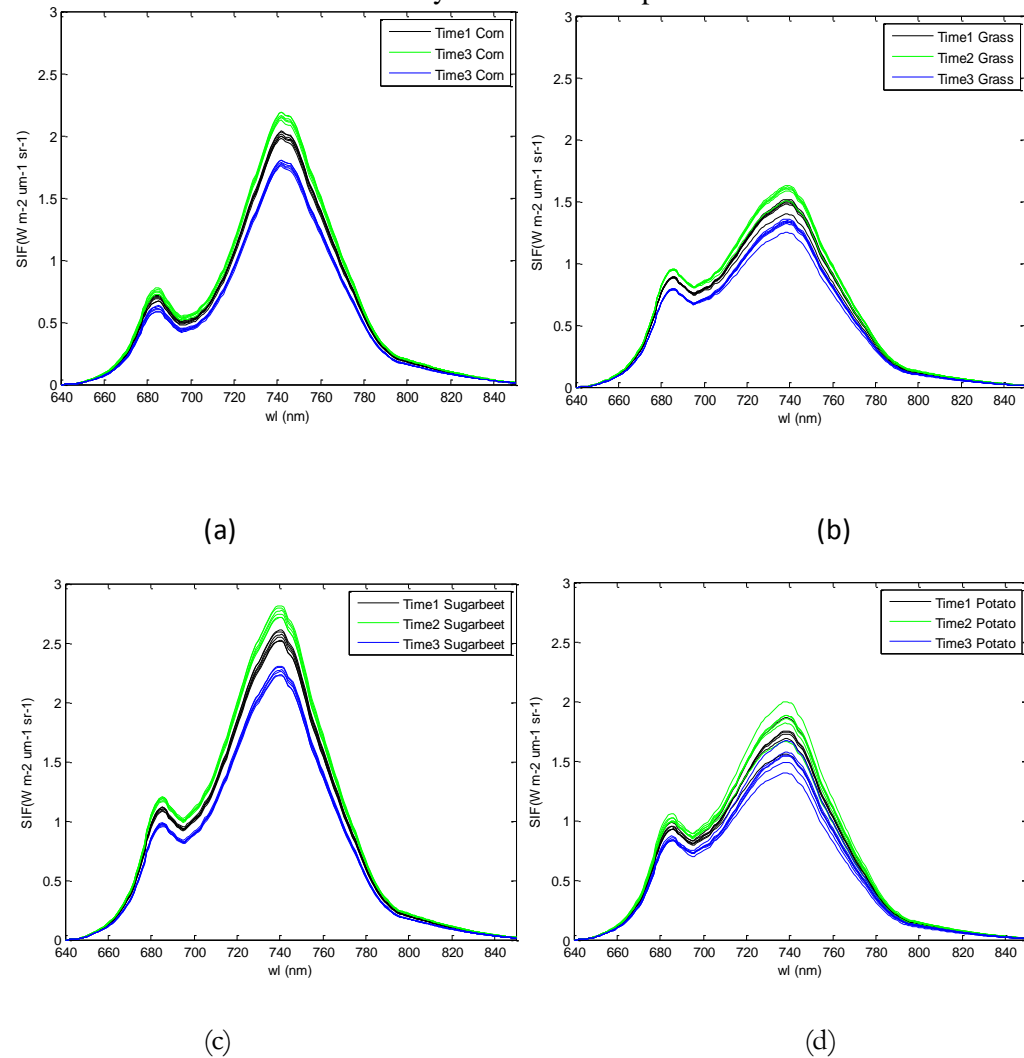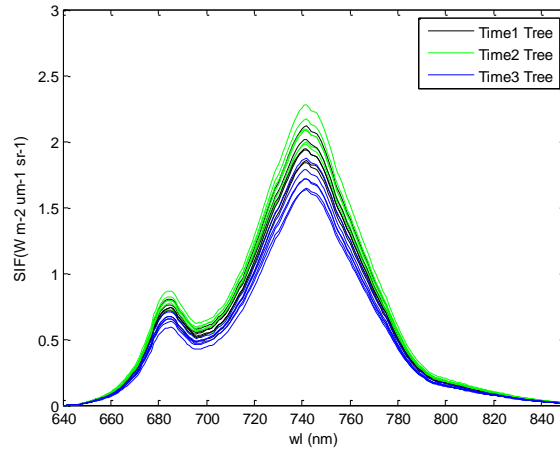
(e)

Figure 17.SIF spectrum of 6 pixels in corn (a), grass (b), sugar beet (c), potato (d) and tree (e) at three local time (time1, 11:56 with black color; time2, 13:50 with green color and time3, 16:05 with blue color).

Figure 18 shows SIF spectra of all five land covers together, one graph for each local time. It can be seen that the shape of the spectra are similar at different local times. Sugar beet have higher position, and peak ratio (F760/F685) of trees and corn is higher than that of grass and potato.
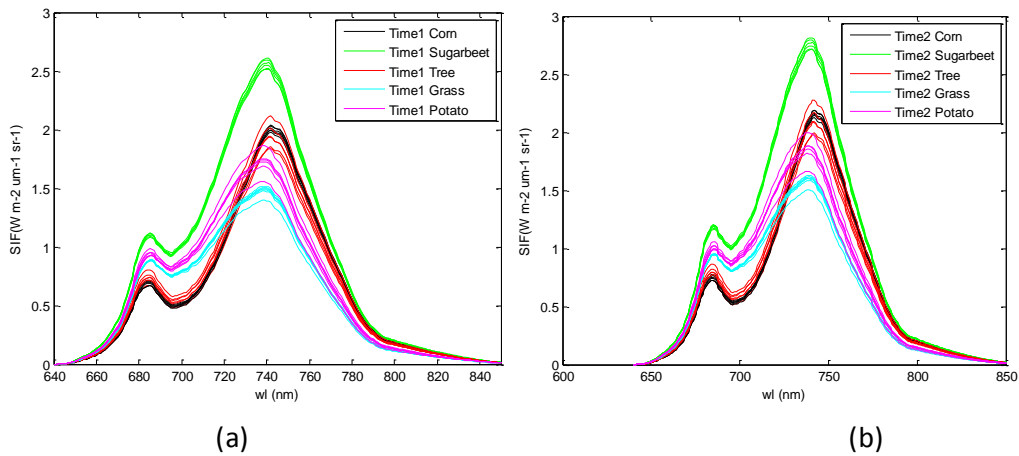
(a)

(b)
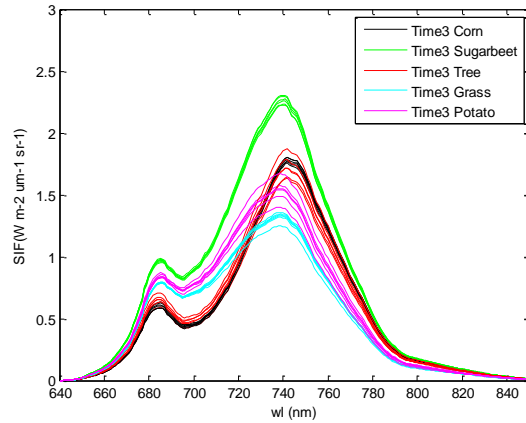
(c)

Figure 18.SIF spectrum of 6 pixels in 5 land cover at 3 local time: time1, 11:56 (a); time2, 13:50 (b) and time3, 16:05 (c).

Linear relations between modelled SIF by SCOPE and HYPLANT measurement SIF at 680, 760 nm were made for all 30 pixels (6 pixels per land cover type) at multiple times in one day, which are 11:56, 13:50 and 16:05 of local time.

For SIF at 680 nm, linear relations between measurement SIF data and simulation SIF data were plotted at different time in Figure 19. Correlation coefficients of linear relations below are 0.0332, 0.2932 and 0.0695 for local time 11:56, 13:50 and 16:05 respectively. Linear relations are not obvious in this case.
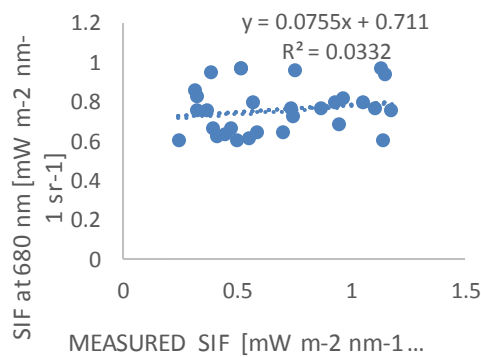
(a)
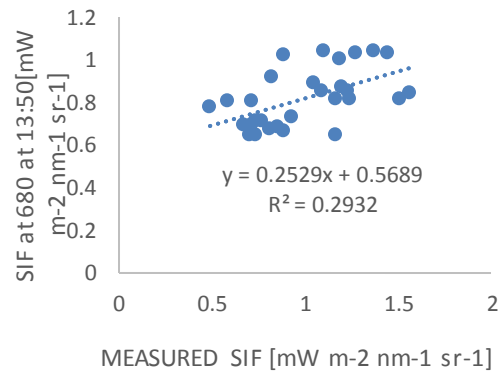
(b)
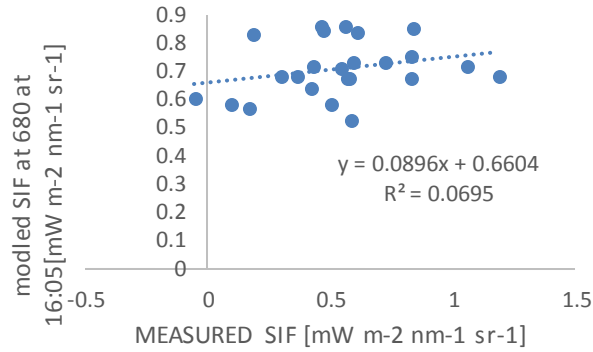
(c)

Figure 19. Linear relations between measured and modelled SIF at 680 nm at 3 times of the day: 11:56 (a); 13:50 (b) and 16:05 (c).

For comparisons of SIF at 760 nm, linear relations between measured SIF and simulated SIF data were also plotted at different time for 24 pixels (6 pixels per land cover type) in Figure 20. In this case, measured SIF data of trees were excluded, because of the occurrence of some (physically impossible) negative values for measured fluorescence. Correlation coefficients of linear relations are 0.63, 0.55 and 0.82 for local time 11:56, 13:50 and 16:05 respectively. Linear correlation coefficients at 760 nm are larger than correlation coefficients at 680 nm. Linear relations are relatively obvious in this case, especially at local time 16:05 with correlation coefficient of 0.82.
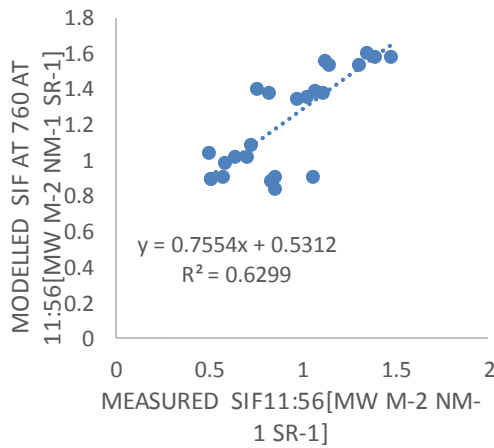
(a)
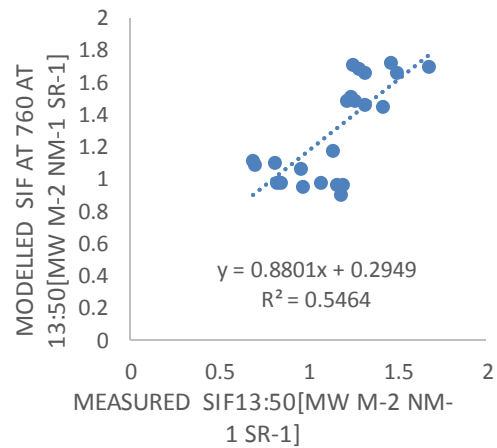
(b)
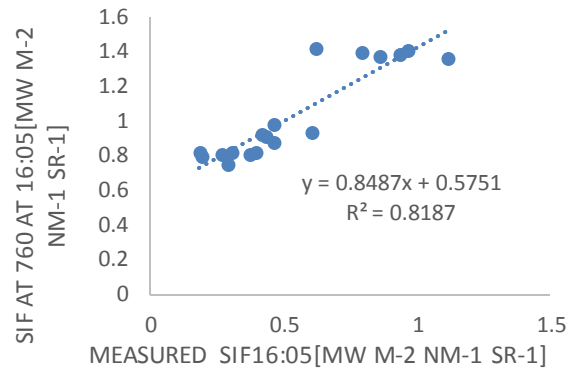
(c)

Figure 20.Linear relations between measured and modelled SIF at 760 nm except trees at 3 local time: time1, 11:56 (a); time2, 13:50 (b) and time3, 16:05 (c).

5.2.   Result of simulation and comparison for transient area

A transient area of adjacent pixels which have relatively obvious trend of decrease of SIF at 760 nm were taken with 18 pixels in sugar beet. Modelled SIF will be used to compare with measurement to check if modelled SIF can represent the measured changing trend.

5.2.1.   Vegetation parameters

By inversion of RTM model, vegetation parameters were retrieved from reflectance for each pixel from NO.1 to NO.18. Chlorophyll content varied 28 to 36 ug cm^{-2} with fluctuation. Water content varied from 0.03 to 0.048 mg cm^{-2} in the similar fluctuation with chlorophyll content. Dry matter content varied from 0.0007 to 0.0021 mg cm^{-2} with different fluctuation pattern. C_s vary from 0.01 to 0.05 (fraction) with frequent fluctuation. C_{ca} vary from 13 to 24 ug cm^{-2} with also different fluctuation pattern. LAI vary from 4.8 to 3.5 (fraction) with relatively simple fluctuation.
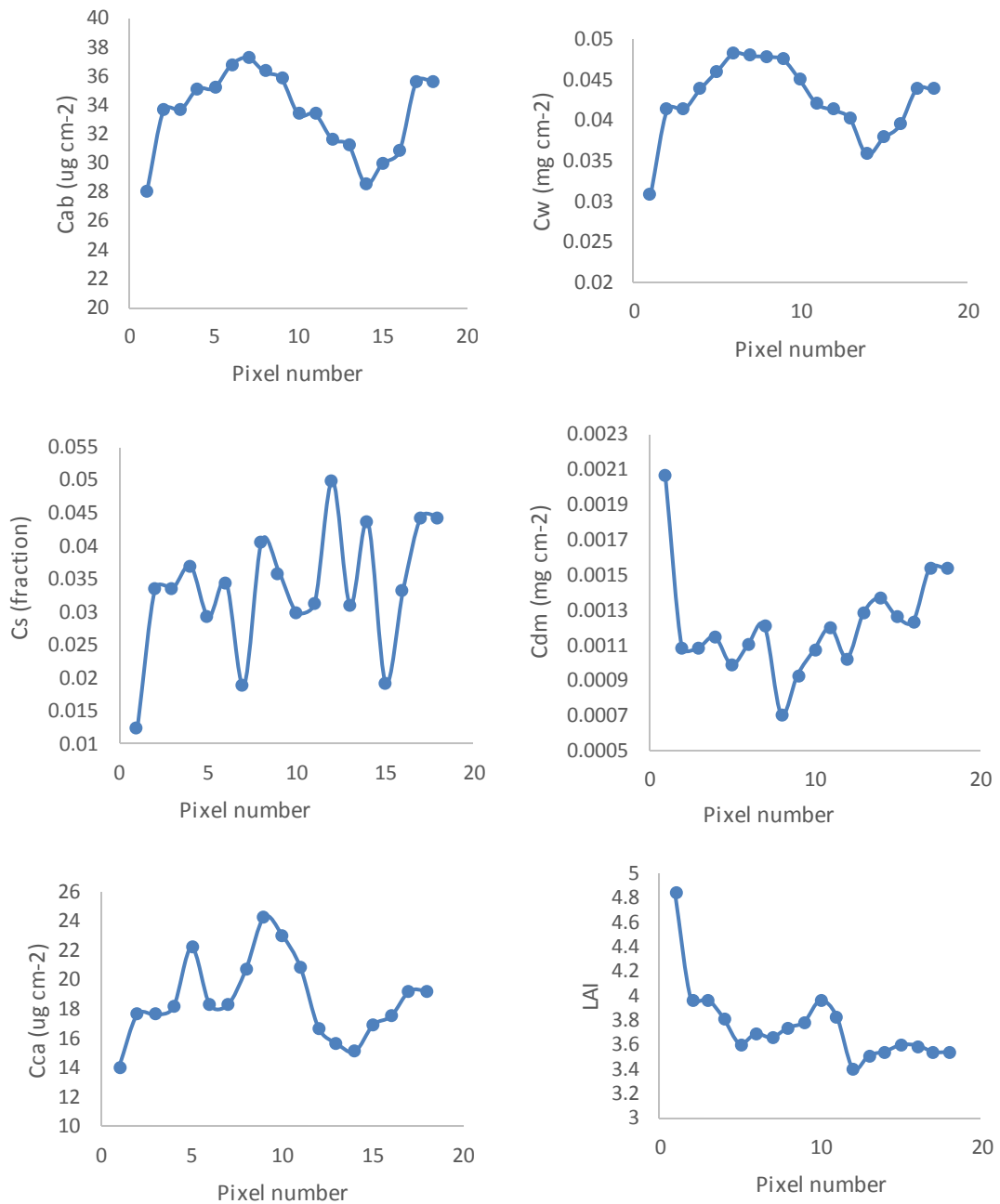
Figure 21. Vegetation parameter changing trend in transient area for C_{ab}, C_w, C_s, C_{dm}, C_{ca} and LAI.

5.2.2. SIF spectrum simulation in transient area

SIF spectra of these 18 pixels were modelled by SCOPE with different vegetation parameters group for each pixel. Spectra from modelling results are shown in Figure 22. From pixel no.1 to no.18, SIF at 760 nm have a trend of small extent decrease. SIF at 680 nm remains nearly the same from pixel no.1 to no.18.
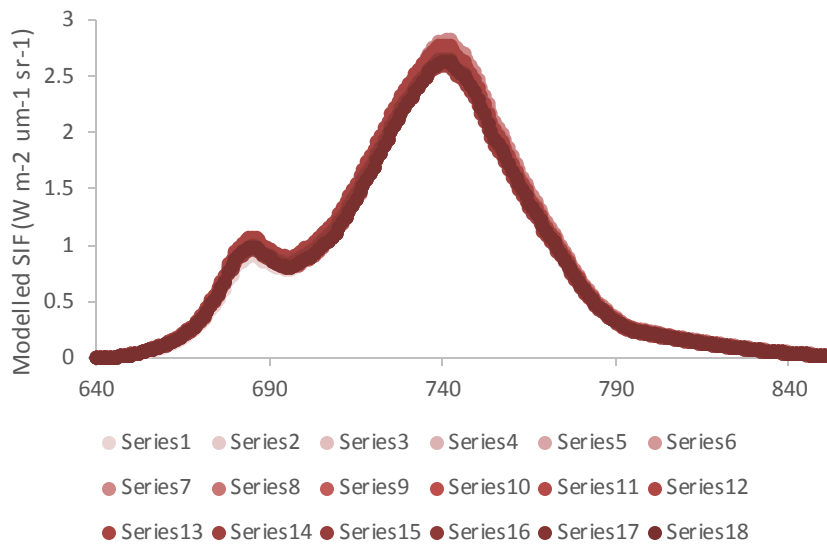
Figure 22. Modelled SIF spectrum by SCOPE for 18 pixels in transient area.

5.2.3. Contrast between modelled and measured SIF in transient area

Figure 23 and Figure 24 show the modelled and measured SIF at two peaks versus pixel number for 18 pixels.

Comparisons between modelled SIF by SCOPE model and HYPLANT measured SIF are plotted at 680 nm in Figure 23. From Figure 23, the extent of variation of measurement SIF at 680 nm are from 0.1 to1.9 W m^{-2} um^{-1} sr^{-1}, while extent of variation of simulated SIF at 680 nm are from 0.86 to 0.94 W m^{-2} um^{-1} sr^{-1}.
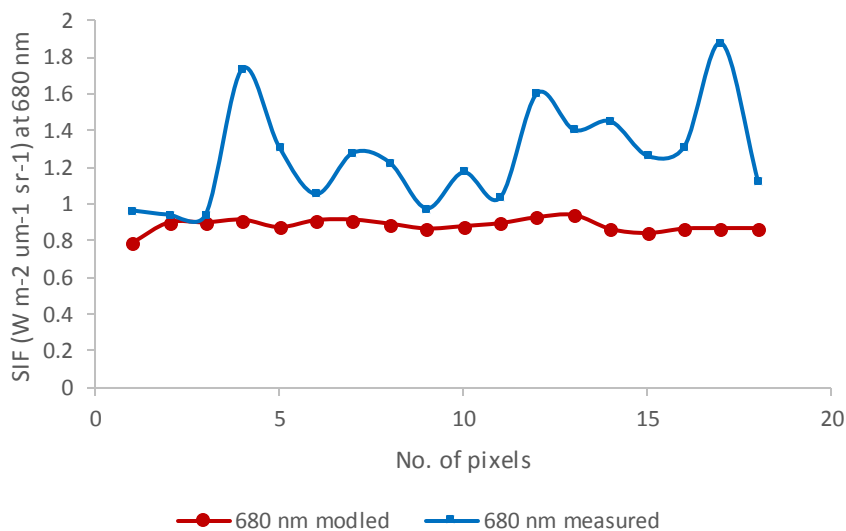
Figure 23.Comparison of modelled and measured SIF of transient area at 680 nm.

Comparisons between modelled SIF by SCOPE model and HYPLANT measured SIF are plotted at 760 nm in Figure 24. From Figure 24, the extent of variation of measurement SIF at 680 nm are from 1.15 to 2.2 W m^{-2} um^{-1} sr^{-1}, while extent of variation of simulated SIF at 680 nm are from 1.6 to 1.8 W m^{-2} um^{-1} sr^{-1}.
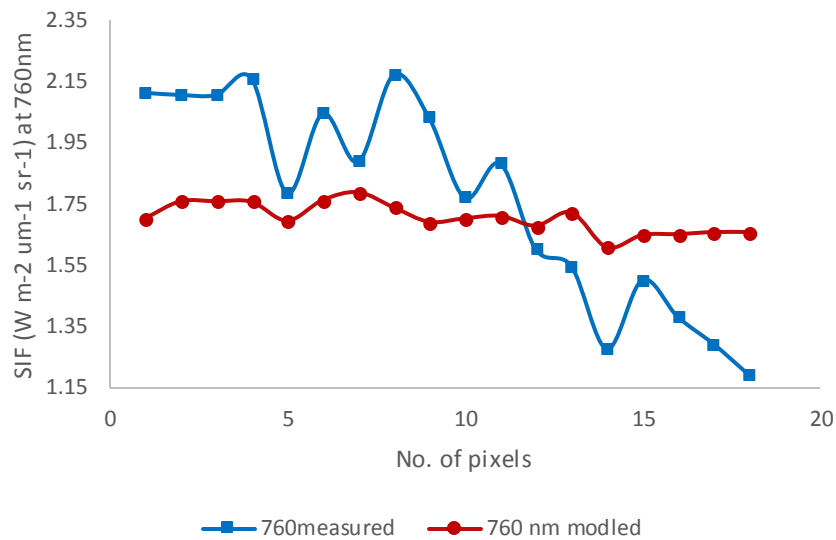
Figure 24.Comparison of modelled and measured SIF of transient area at 760 nm.

6. ANALYSIS

6.1. Systematic error

There can be random errors and systematic errors for model results. If the model has some deficiencies, systematic errors may come to result. In this case, systematic error could appear in the simulated result of all vegetation types. During vegetation parameters retrieval process, calibration of model was done by minimize differences (Root mean square error, RMSE) between measured and modelled reflectance spectrum. Difference of simulated and measured spectrum of one pixel in sugar beet is in Figure 25. Normally, RMSE in result of each pixel was approximately 0.014.
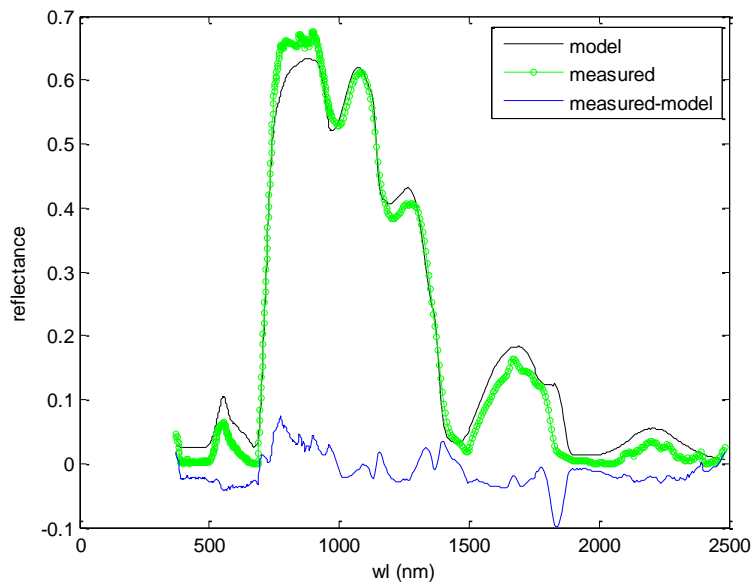
Figure 25. Simulation result of one pixel of sugar beet.
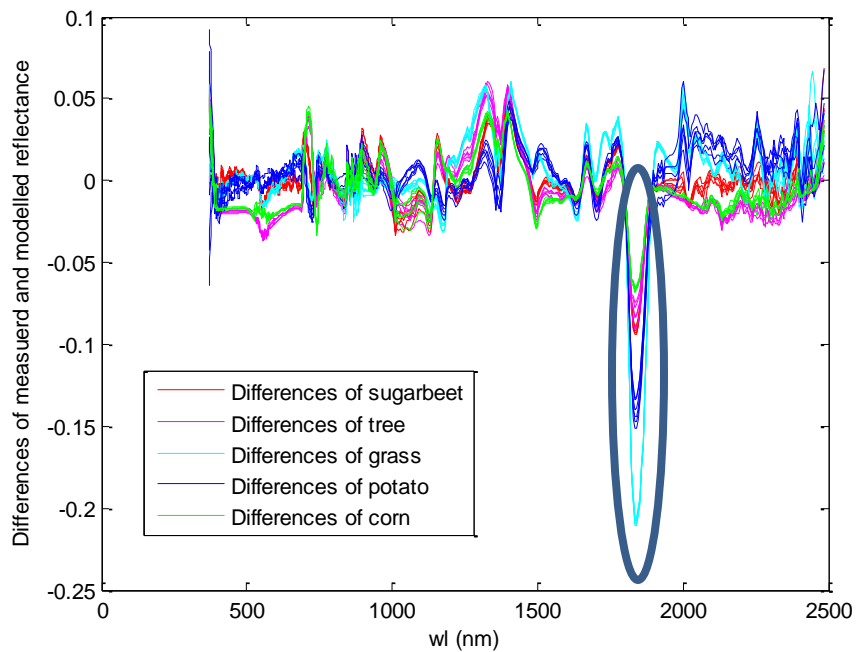
Figure 26. Spectral differences between measured and modelled reflectance of each 6 pixels in sugar beet, tree, grass, potato and corn.

Differences (measured-modelled) between measured and modelled spectra for different land cover were shown in Figure 26. In the region which been marked in blue, measured reflectance are lower than modelled reflectance in all land cover types and

pixel samples. The possible reason of this systematic error, could be either model deficiencies or uncertainties in the processing of measurements, such as atmosphere correction of reflectance. Obviously it is water vapor absorption band in the blue region. Then another possible explanation is that water vapor's atmospheric correction has some uncertainty in this reflectance data. Further study is needed.

6.2. SIF's spatial variability feature in HYPLANT

6.2.1. SIF's variability feature in HYPLANT of different vegetation types

SIF data in HYPLANT include two wavelength which are 680 and 760 nm. From the view of relatively large spatial scale, SIF data of image from HYPLANT have obvious variability with different vegetation types. In Figure 27, SIF data's distribution for different vegetation types (grass, corn, potato and sugar beet) were made at 680 and 760 nm with subclass2 of dataset 1. In Subclass 2, corn, tree, grass, sugar beet and potato have 418 pixels, 240 pixels, 504 pixels, 672 pixels and 192 pixels respectively. This subclass data are used to analyze variability of SIF for different land cover. It can be concluded that SIF of these vegetation types have some specific distribution features in the plot, especially for sugar beet.

Data of SIF from tree were included with other vegetation types together in Figure 28. It can be seen that SIF distributions of tree have some overlap with grass, corn and potato, especially with corn.
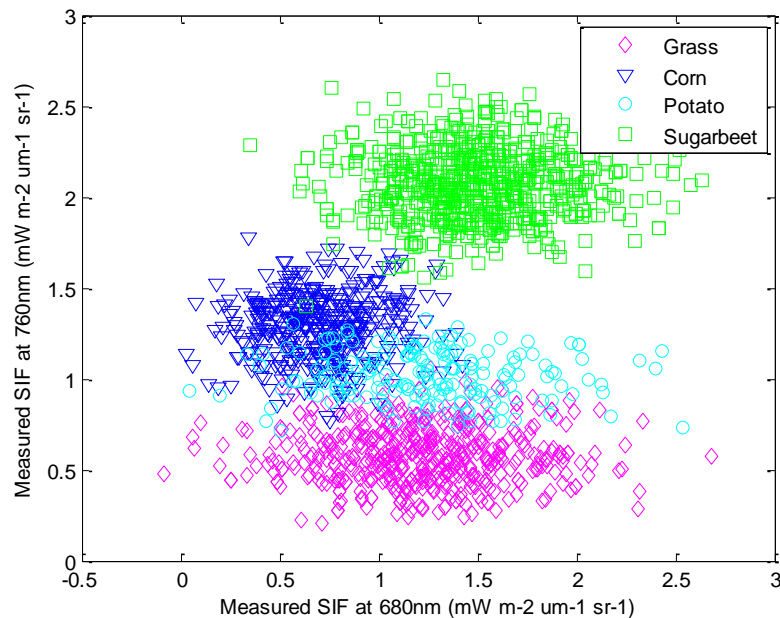
Figure 27.HYPLANT SIF data's distribution for different vegetation types (grass, corn, potato and sugar beet) at 680 and 760 nm.
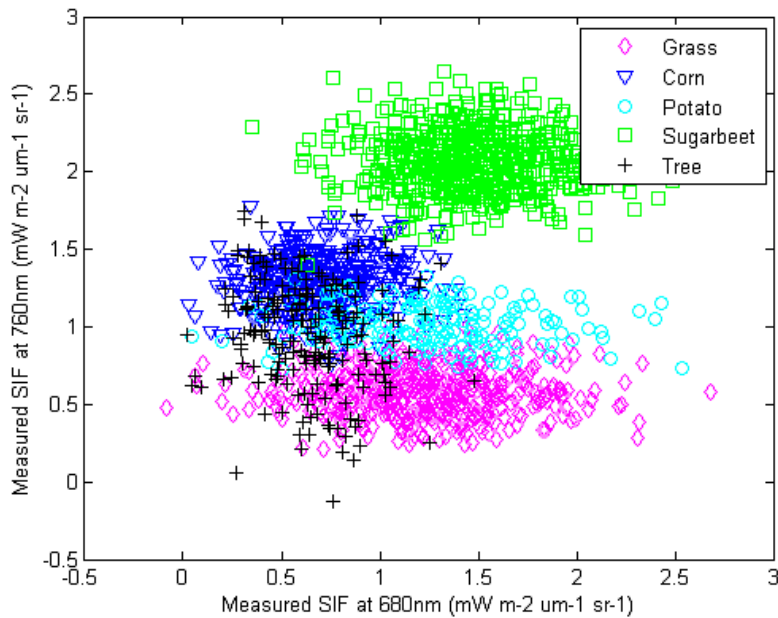
Figure 28.HYPLANT SIF data's distribution for different vegetation types (grass, corn, potato, sugar beet and tree) at 680 and 760 nm.

6.2.2. SIF's variability feature in transient area in HYPLANT

Measured SIF data at 760 nm show rather large spatial variability at small spatial scale (adjacent pixels of 1 m resolution). The corresponding changing trend of SIF at 680 can be shown by comparing SIF changing trend at 760 nm and at 680 nm.

In Figure 29, SIF data at 760 nm and 680 nm were plotted, and pixel were sorted in descending order of SIF at 760 nm with subclass2 of dataset2. In Subclass 2, 348 pixels with relatively obvious changing SIF at 760 nm inside sugar beet field were chosen. After sorting, SIF at 760 nm have obvious drop from 2.8 to 1.6 mW m^{-2} um^{-1} sr^{-1}, while SIF at 680 nm have frequent fluctuations and do not have obvious variation trend. It can be concluded that changing trend of SIF at 680nm are different from changing trend of SIF at 760nm.
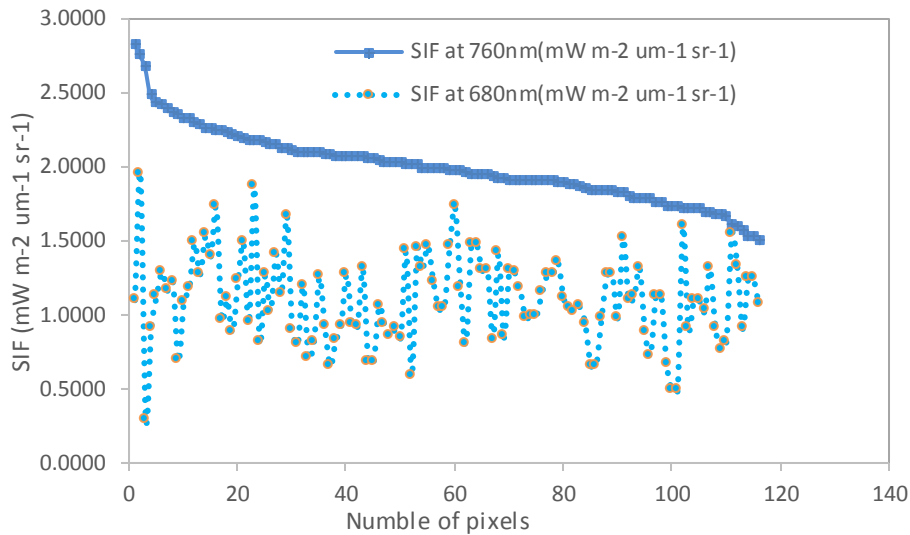
Figure 29.HYPLANT SIF data's distribution for transient area (sugar beet) at 680 and 760 nm.

6.3. Analysis of comparison results

6.3.1. Analysis of comparison results for different vegetation types

From results in Modelled SIF spectrum and comparison at noon5.1.2, it is clear that variations of modelled SIF are smaller than measured for general situation both at 680 and 760 nm. Also, there are differences of modelling result for multiple vegetation types.

For comparisons of SIF at 680 nm, linear relations were built for different vegetation types to check effects of simulation results. Linear correlation coefficients are 0.20, 0.75, 0.61, 0.21 and 0.10 respectively for corn, grass, potato, sugar beet and tree. Relations for grass with relatively high coefficient were resented in Figure 30. It can also be seen that modelled SIF can present similar trend with measured SIF at 680 nm for samples of grass, but the variations of modelled SIF are much lower than measured.

For comparisons of SIF at 760 nm, linear relations were also built for different vegetation types to check effects of simulation results. Linear coefficients are 0.87, 0.31, 0.01, 0.02 and 0.97 respectively for corn, grass, potato, sugar beet and tree. Relations for tree with relatively high coefficient were resented in Figure 31. It can be seen that modelled SIF can present very similar trend with measured SIF at 760 for samples of tree, but again the variations of modelled SIF are also much lower than measured.
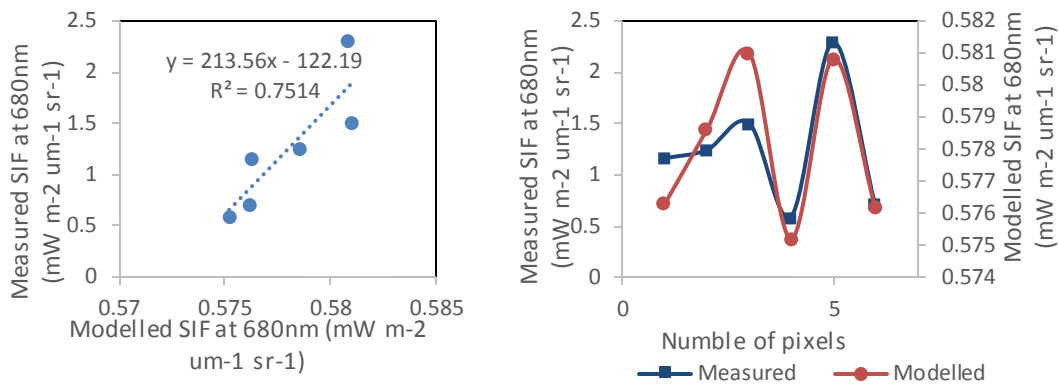
Figure 30.Relation between modelled and measured SIF at 680 nm for grass.

Figure 31.Relation between modelled and measured SIF at 760 nm for tree.

6.3.2. Analysis of comparison results for transient area

From results in Modelled SIF spectrum and comparison at noon5.2.3, variations of modelled SIF in transient area are smaller than measured both at 680 and 760 nm. However there are some similar trend between the curve of measured and curve of modelled SIF both at 680 nm and 760 nm with 18 samples from sugar beet. This can be seen when plotting the simulated and measured data over the transient each on a different y-axis.

For comparisons of SIF at 680 nm in transient area, comparison was built for to check effects of simulation results. From Figure 32 and Figure 34, it can be concluded that the variations of modelled SIF are much lower than measured, and linear relation between measured and modelled SIF is low.

For comparisons of SIF at 760 nm in transient area, comparison was also built for to check the effects of simulation results. In Figure 33 and Figure 34, it can be seen that modelled SIF can present some more obvious similar changes with measured SIF at 760nm than modelling at 680 nm, also the linear relation is more obvious. But the variations of modelled SIF are still much lower than measured.

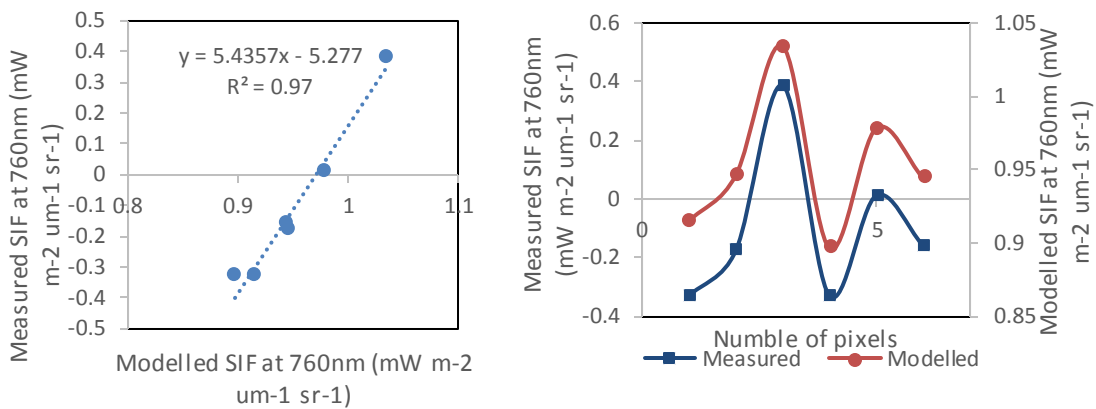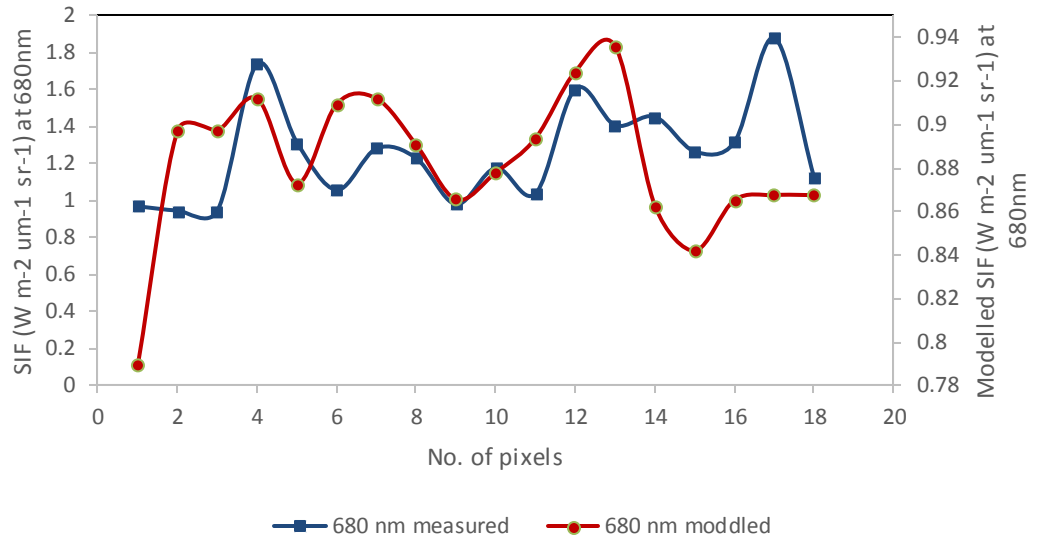Figure 32.Relation between modelled and measured SIF of transient area at 680 nm.
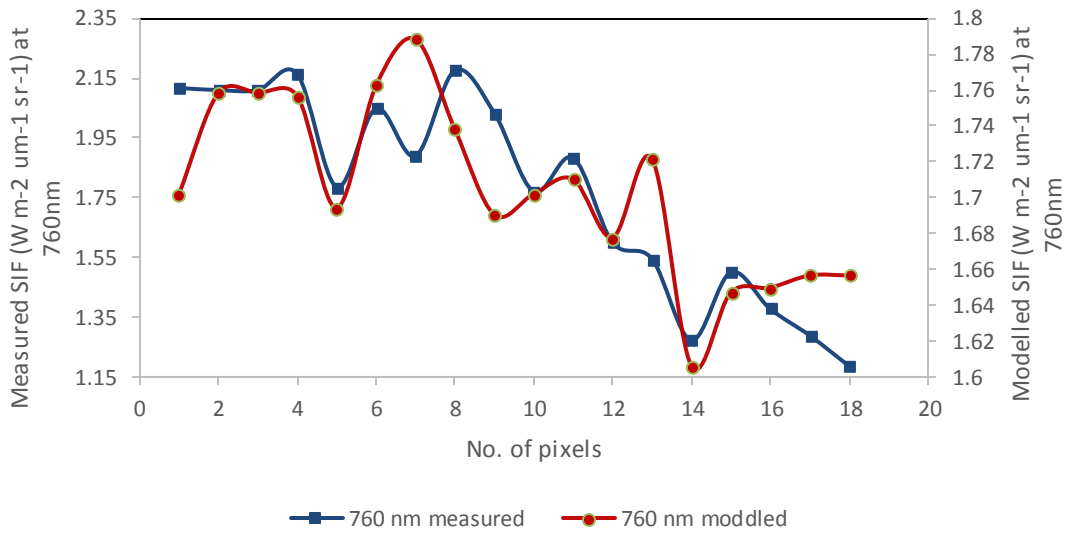
Figure 33.Relation between modelled and measured SIF of transient area at 760 nm.
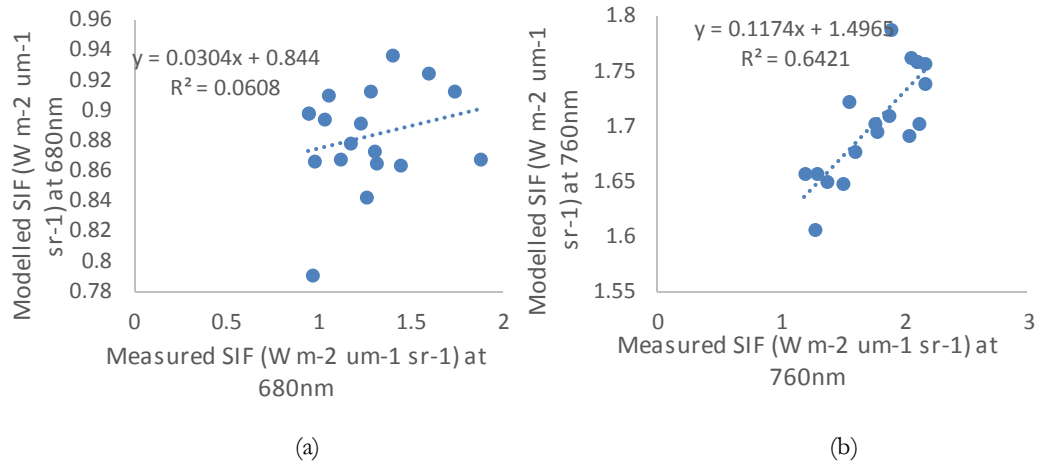
Figure 34. Correlations between measured and modelled SIF at 680 (a) and 760 nm (b).

7. CONCLUSION AND RECOMMENDATIONS

7.1. The added value of fluorescence

Nearly all the modelled SIF are different with HYPLANT measurements at 680 and 760 nm. Correlation coefficients between modelled and measured SIF for general cases are lower than 0.7. Correlation coefficients at 680 nm are lower than Correlation coefficients at 760 nm for most situations. Generally, SIF modelling at 760 nm have better performance than SIF modelling at 680 nm. Still, it can be concluded that measured and modelled fluorescence have low linear relations, especially for SIF at 680 nm.

Variations of modelled SIF are smaller than measured for general situation both at 680 and 760 nm. Only in some cases, modelled can represent similar changing trend with measured SIF. So measured SIF are more sensitive to plant than modelled SIF from reflectance. Variations of fluorescence signal can represent changes in vegetation growing condition, based on relation between fluorescence and GPP for example (Luis Guanter, Zhang, Jung, Joiner, Voigt, et al., 2014). Large variations of SIF may result relatively more variations in GPP. Then additional information in GPP can be indicated by using measured fluorescence in theory.

Because of low relations between modelled and measured SIF, especially for SIF at 680 nm, additional information of measured SIF are not easy to be obtained by modelled SIF from reflectance.

Therefore the added value of SIF can be concluded as follow:

SIF are unique compared to reflectance data.

SIF are more sensitive to plant than reflectance, and it can provide more additional information about Vegetation conditions, such as GPP of plant.

7.2. Spatial variability feature of SIF in HYPLANT data

For different vegetation types, there are certain and specific distribution features for different land covers in SIF plot (SIF at 680 nm versus SIF at 760 nm), especially for sugar beet. But tree's SIF distributions in the plot have some overlap with grass, corn and potato.

For transient area, SIF at 760 nm have big decrease after sorting while SIF at 680 nm remain frequent fluctuations in random way. It can be analyzed that SIF at 680nm and 760nm do not have similar changing trend, in this case.

7.3. Recommendations

In this research, Systematic errors were found in vegetation parameter retrieval process which may bring errors to SIF simulation through vegetation parameters. The reason could be either model deficiencies or uncertainties in the processing of measurements, such as atmosphere correction of reflectance.

V_{cmo} which can have influences in photosynthetic efficiency, were kept at default value in this research because of lack of measurements of V_{cmo}. This may reduce accuracy in SIF simulation results.

So for further researches, there are two issues needed to pay attention which are possible ways to reduce systematic errors of vegetation parameters retrieval and parameter V_{cmo}' effects to SIF simulation.

REFERENCES

Baker, N. R. (2008). Chlorophyll fluorescence: a probe of photosynthesis in vivo. *Annual Review of Plant Biology*, *59*, 89–113. http://doi.org/10.1146/annurev.arplant.59.032607.092759

Bréda, N. J. J. (2003). Ground-based measurements of leaf area index: a review of methods, instruments and current controversies. *Journal of Experimental Botany*, *54*(392), 2403–17. http://doi.org/10.1093/jxb/erg263

Butler, W. L. (1978). Energy Distribution in the Photochemical Apparatus of Photosynthesis. *Annual Review of Plant Physiology*, *29*(1), 345–378. http://doi.org/10.1146/annurev.pp.29.060178.002021

Caicedo, J. P. R., Verrelst, J., Munoz-Mari, J., Moreno, J., & Camps-Valls, G. (2014). Toward a Semiautomatic Machine Learning Retrieval of Biophysical Parameters. *IEEE Journal of Selected Topics in Applied Earth Observations and Remote Sensing*, *7*(4), 1249–1259. http://doi.org/10.1109/JSTARS.2014.2298752

Cowling, S. A., & Field, C. B. (2003). Environmental control of leaf area production: Implications for vegetation and land-surface modeling. *Global Biogeochemical Cycles*, *17*(1), 7–1–7–14. http://doi.org/10.1029/2002GB001915

Frankenberg, C., Fisher, J. B., Worden, J., Badgley, G., Saatchi, S. S., Lee, J. E., … Yokota, T. (2011). New global observations of the terrestrial carbon cycle from GOSAT: Patterns of plant fluorescence with gross primary productivity. *Geophysical Research Letters*, *38*(17), 1–6. http://doi.org/10.1029/2011GL048738

G.seaton, & D.walker. (1990). Chlorophyll fluorescence as a measure of photosynthetic carbon assimilation.

Gitelson, A. a., Peng, Y., Arkebauer, T. J., & Schepers, J. (2014). Relationships between gross primary production, green LAI, and canopy chlorophyll content in maize: Implications for remote sensing of primary production. *Remote Sensing of Environment*, *144*, 65–72. http://doi.org/10.1016/j.rse.2014.01.004

Guanter, L., Alonso, L., Gómez-Chova, L., Meroni, M., Preusker, R., Fischer, J., & Moreno, J. (2010). Developments for vegetation fluorescence retrieval from spaceborne high-resolution spectrometry in the O2-A and O2-B absorption bands. *Journal of Geophysical Research: Atmospheres*, *115*(19). http://doi.org/10.1029/2009JD013716

Guanter, L., Zhang, Y., Jung, M., Joiner, J., & Voigt, M. (2014). Global and time-resolved monitoring of crop photosynthesis with chlorophyll fluorescence. Retrieved August 22, 2015, from http://www.biometeorology.umn.edu/pdf/guanter2014.pdf

Guanter, L., Zhang, Y., Jung, M., Joiner, J., Voigt, M., Berry, J. a, … Griffis, T. J. (2014). Global and time-resolved monitoring of crop photosynthesis with chlorophyll

fluorescence. *Proceedings of the National Academy of Sciences of the United States of America*, *111*(14), E1327–33. http://doi.org/10.1073/pnas.1320008111

Houborg, R., Anderson, M. C., Daughtry, C. S. T., Kustas, W. P., & Rodell, M. (2011). Using leaf chlorophyll to parameterize light-use-efficiency within a thermal-based carbon, water and energy exchange model. *Remote Sensing of Environment*, *115*(7), 1694–1705. http://doi.org/10.1016/j.rse.2011.02.027

Houborg, R., Cescatti, A., & Migliavacca, M. (2012). Constraining model simulations of GPP using satellite retrieved leaf chlorophyll. *2012 IEEE International Geoscience and Remote Sensing Symposium*, 6455–6458. http://doi.org/10.1109/IGARSS.2012.6352741

J. L. Monteith. (1997). Solar Radiation and Productivity in Tropical Ecosystems. Retrieved January 30, 2016, from http://www.jstor.org/stable/2401901?seq=1#page_scan_tab_contents

Jacquemoud, S., & Baret, F. (1990a). PROSPECT: A model of leaf optical properties spectra. *Remote Sensing of Environment*, *34*(2), 75–91. http://doi.org/10.1016/0034-4257(90)90100-Z

Jacquemoud, S., & Baret, F. (1990b). PROSPECT: A model of leaf optical properties spectra. *Remote Sensing of Environment*, *34*(2), 75–91. http://doi.org/10.1016/0034-4257(90)90100-Z

Jacquemoud, S., Verhoef, W., Baret, F., Bacour, C., Zarco-Tejada, P. J., Asner, G. P., … Ustin, S. L. (2009). PROSPECT + SAIL models: A review of use for vegetation characterization. *Remote Sensing of Environment*, *113*(SUPPL. 1), S56–S66. http://doi.org/10.1016/j.rse.2008.01.026

Jiang, C., & Hongliang, F. (2012). MODELING SOIL REFLECTANCE USING A GLOBAL SPECTRAL LIBRARY. *AGU*.

Joiner, J., Guanter, L., Lindstrot, R., Voigt, M., Vasilkov, a P., Middleton, E. M., … Frankenberg, C. (2013). Global monitoring of terrestrial chlorophyll fluorescence from moderate spectral resolution near-infrared satellite measurements: methodology, simulations, and application to GOME-2. *Atmospheric Measurement Techniques Discussions*, *6*(2), 3883–3930. http://doi.org/10.5194/amtd-6-3883-2013

Kattge, J., Knorr, W., Raddatz, T., & Wirth, C. (2009). Quantifying photosynthetic capacity and its relationship to leaf nitrogen content for global-scale terrestrial biosphere models. *Global Change Biology*, *15*(4), 976–991. http://doi.org/10.1111/j.1365-2486.2008.01744.x

Krause, G. H., & Jahns, P. (2004). *Non-photochemical Energy Dissipation Determined by Chlorophyll Fluorescence Quenching: Characterization and Function*. (G. C. Papageorgiou, Ed.) (Vol. 19). Dordrecht: Springer Netherlands. http://doi.org/10.1007/978-1-4020-3218-9

Le Maire, G., François, C., & Dufrêne, E. (2004). Towards universal broad leaf chlorophyll indices using PROSPECT simulated database and hyperspectral reflectance measurements. *Remote Sensing of Environment*, *89*(1), 1–28. http://doi.org/10.1016/j.rse.2003.09.004

Meroni, M., Rossini, M., Guanter, L., Alonso, L., Rascher, U., Colombo, R., & Moreno, J. (2009). Remote sensing of solar-induced chlorophyll fluorescence: Review of methods and applications. *Remote Sensing of Environment*, *113*(10), 2037–2051. http://doi.org/10.1016/j.rse.2009.05.003

Mutanga, O., Adam, E., & Cho, M. A. (2012). High density biomass estimation for wetland vegetation using WorldView-2 imagery and random forest regression algorithm. *International Journal of Applied Earth Observation and Geoinformation*, *18*, 399–406. http://doi.org/10.1016/j.jag.2012.03.012

Pedrós, R., Goulas, Y., Jacquemoud, S., Louis, J., & Moya, I. (2010). FluorMODleaf: A new leaf fluorescence emission model based on the PROSPECT model. *Remote Sensing of Environment*, *114*(1), 155–167. http://doi.org/10.1016/j.rse.2009.08.019

Peng, Y., Gitelson, A. A., Keydan, G., Rundquist, D. C., & Moses, W. (2011). Remote estimation of gross primary production in maize and support for a new paradigm based on total crop chlorophyll content. *Remote Sensing of Environment*, *115*(4), 978–989. http://doi.org/10.1016/j.rse.2010.12.001

Rascher, U., Alonso, L., Burkart, a., Cilia, C., Cogliati, S., Colombo, R., … Zemek, F. (2015). Sun-induced fluorescence - a new probe of photosynthesis: First maps from the imaging spectrometer *HyPlant*. *Global Change Biology*, (0), n/a–n/a. http://doi.org/10.1111/gcb.13017

Sage, R. F., & Pearcy, R. W. (1987). The Nitrogen Use Efficiency of C3 and C4 Plants: II. Leaf Nitrogen Effects on the Gas Exchange Characteristics of Chenopodium album (L.) and Amaranthus retroflexus (L.). *PLANT PHYSIOLOGY*, *84*(3), 959–963. http://doi.org/10.1104/pp.84.3.959

Tilman, D., Balzer, C., Hill, J., & Befort, B. L. (2011). From the Cover: Global food demand and the sustainable intensification of agriculture. *Proceedings of the National Academy of Sciences*, *108*(50), 20260–20264. http://doi.org/10.1073/pnas.1116437108

Van Der Tol, C., Rossini, M., Rascher, U., Verhoef, W., & Mohammed, G. (2016). A model and measurement comparison of diurnal cycles of sun induced chlorophyll fluorescence of crops, 1–13.(submitted)

Van der Tol, C., Verhoef, W., Timmermans, J., Verhoef, a., & Su, Z. (2009). An integrated model of soil-canopy spectral radiances, photosynthesis, fluorescence, temperature and energy balance. *Biogeosciences*, *6*(12), 3109–3129. http://doi.org/10.5194/bg-6-3109-2009

Verhoef, W. (1984). Light scattering by leaf layers with application to canopy reflectance modeling: The SAIL model. *Remote Sensing of Environment*, *16*(2), 125–141. http://doi.org/10.1016/0034-4257(84)90057-9

Verhoef, W., Tol, C. Van Der, & Middleton, E. M. (2014). Vegetation Canopy Fluorescence and Reflectance Retrieval By Model Inversion Using Optimization. *5th International Workshop on Remote Sensing of Vegetation Fluorescence*, (1), 759–770. Retrieved from http://congrexprojects.com/Custom/14C04/14C04_index.htm

Verrelst, J., Camps-Valls, G., Muñoz-Marí, J., Rivera, J. P., Veroustraete, F., Clevers, J. G. P. W., & Moreno, J. (2015). Optical remote sensing and the retrieval of terrestrial vegetation bio-geophysical properties - A review. *ISPRS Journal of Photogrammetry and Remote Sensing*, *108*, 273–290. http://doi.org/10.1016/j.isprsjprs.2015.05.005

Verrelst, J., Rivera, J. P., van der Tol, C., Magnani, F., Mohammed, G., & Moreno, J. (2015). Global sensitivity analysis of the SCOPE model: What drives simulated canopy-leaving sun-induced fluorescence? *Remote Sensing of Environment*, *166*, 8–21. http://doi.org/10.1016/j.rse.2015.06.002

Viña, A., Gitelson, A. A., Nguy-Robertson, A. L., & Peng, Y. (2011). Comparison of different vegetation indices for the remote assessment of green leaf area index of crops. *Remote Sensing of Environment*, *115*(12), 3468–3478. http://doi.org/10.1016/j.rse.2011.08.010